



Assessing the Sources of Submicron Airborne Elements at two sites in the Fos-Marseille Basin through Rolling Positive Matrix Factorization

Mathilde Brezins¹, Benjamin Chazeau¹, Nicolas Marchand¹, Amandine Durand¹, Grégory Gille²,
5 Romain Bourjot², Andre S.H. Prévôt³, Jean-Luc Jaffrezo⁴, Gaëlle Uzu⁴ and Barbara D'Anna¹

¹Aix Marseille Univ, CNRS, LCE, Marseille, 13331, France

²AtmoSud, Regional Network for Air Quality Monitoring of Provence-Alpes-Côte-d'Azur, Marseille, France

³Laboratory of Atmospheric Chemistry, Paul Scherrer Institute, 5232 Villigen, Switzerland

⁴Univ. Grenoble Alpes, CNRS, IRD, INP, IGE (UMR 5001), 38000 Grenoble, France

10

Correspondence to: Benjamin Chazeau (benjamin.chazeau@univ-amu.fr), Barbara D'Anna (barbara.danna@univ-amu.fr)

Abstract.

Contributions and evolution of fine elemental particulate matter (PM) sources were investigated in the Marseille-Fos basin
15 (South of France) based on a 1 year-long (January-December 2023) study using on-line x-ray fluorescence (Xact) PM₁
measurements. The region's intense anthropogenic activity and complex meteorological conditions make it an ideal case
study for fine aerosol characterization. Given the limited information available on fine elemental sources in the area, a dual-
site approach was implemented, combining an urban background site (MRS-LCP) and an industrial site (FOS) to distinguish
between regional and local emission influences. Source apportionment was conducted using a rolling Positive Matrix
20 Factorization (PMF) method, implemented via the Source Finder Professional (SoFi) toolkit. Several tests were carried out to
determine optimal rolling PMF parameters. Eventually, a 21-day rolling window configuration was selected, resolving nine
factors at FOS and eight at MRS-LCP, with seven similar factors detected at both sites. Among them, three were attributed
to secondary aerosols, including sulfur photooxidation leading to sulfate-rich aerosols (S-rich factor) and the formation of
halogenated reactive particulate species (Cl-rich and Br-rich factors). Additionally, biomass burning, shipping, and dust
25 related factors were identified at both locations. In contrast, three industrial factors (Steel Industry, Zn-Industrial, Pb-
Industrial) were detected at FOS, while only the Steel Industry factor appeared at MRS-LCP, suggesting downwind transport
of industrial plumes from Fos-sur-Mer to Marseille under Mistral and thermal breeze regimes. Furthermore, the comparison
of dynamic rolling PMF approach to static PMF analysis, demonstrated higher dissimilarities across factors profiles,
reflecting enhanced ability of Rolling PMF to capture seasonal variability in aerosol sources. Overall, this study highlights
30 the dominant anthropogenic imprint on submicron PM elements and the effectiveness of dynamic source apportionment in
complex coastal-industrial environments.



1 Introduction

Air pollution has long been recognized as a major threat to human health (Dockery et al., 1993), representing the leading environmental risk factor for premature mortality globally and the second leading overall risk factor for death (WHO, 2021). Fuller et al. (2022) estimated it was responsible for 9 million premature deaths per year worldwide. Intensified anthropogenic activities, particularly urbanization, industrialization, and widespread fossil fuel use, further degrade air quality, presenting a double jeopardy as they impact both human health and the climate system (Schmale et al., 2014). In a context of rapid climate change, understanding the complex interplay of aerosols is crucial, as climate change may further increase aerosol production (e.g., more frequent Saharan dust outbreaks, increased wildfire episodes, and volatile organic compound emissions from stressed vegetation) (Gomez et al., 2022; Bourtsoukidis et al., 2024; Pons et al., 2025). Climate change hot spots such as the Mediterranean Basin are particularly at risk, with projections indicating more frequent and intense meteorological extremes that could trigger additional pollution episodes (Zittis et al., 2022; Jézéquel et al., 2025).

The city of Marseille (France) embodies these vulnerabilities. With its dense population and exposure to numerous pollution sources, it represents a highly complex and dynamic atmospheric environment. Anthropogenic activities in the region include one of the largest ports in the Mediterranean Sea, and major industrial facilities. In particular, industrial sites located in the north-western suburbs of the Marseille-Fos basin are recognized contributors to Marseille's air pollution (El Haddad et al., 2013; Salameh et al., 2018; Chazeau et al., 2021). The diversity of pollution sources, combined with local meteorological conditions, such as frequent land-sea breeze circulations, favour the ageing and formation of secondary aerosols (Puygrenier et al., 2005; Drobinski et al., 2007), effectively transforming the Marseille basin into a chemical reactor for atmospheric particles. This complexity has drawn significant scientific attention to the region (Bozetti et al., 2017; Chevet et al., 2024; Dufresne et al., 2025). In particular, fine particulate matter smaller than 1 μm (PM_{10}) is a major health concern, due to its ability to penetrate deeply into the respiratory system (Kreyling et al., 2006), but it remains unregulated in France. Consequently, submicron aerosol composition and dynamics in the Marseille area have attracted growing scientific interest in recent years (El Haddad et al., 2013; Chazeau et al., 2021; Camman et al., 2024; Le Berre et al., 2025).

While several studies have characterized the organic fraction of submicron aerosols in Marseille (Haddad et al., 2013; Bozetti et al., 2017; Chazeau et al., 2022), source apportionment of airborne elements, including non-metals, metals and metalloids, remains scarce (Camman et al., 2024). This is critical, as many metallic elements such as Pb, Hg, As, Cr, Ni, and Cd are found to be toxic, bioaccumulative, and associated with carcinogenic, neurotoxic, or cardiovascular effects (Rose, 1983). Recent advances in automated, high-time-resolution energy-dispersive X-ray fluorescence (ED-XRF) instrumentation (e.g., Xact 625i, Cooper Environmental Services) allow continuous, highly-time resolved measurements of a wide range of airborne elements (Furger et al., 2017; Tremper et al., 2018), offering new opportunities to assess airborne elements source dynamics and temporal variability.

In this study, we aim to identify and characterize the sources of submicron airborne elements in the Marseille-Fos basin using the whole 2023 year of high-time resolution Xact measurement data. To capture temporal variability in source profiles

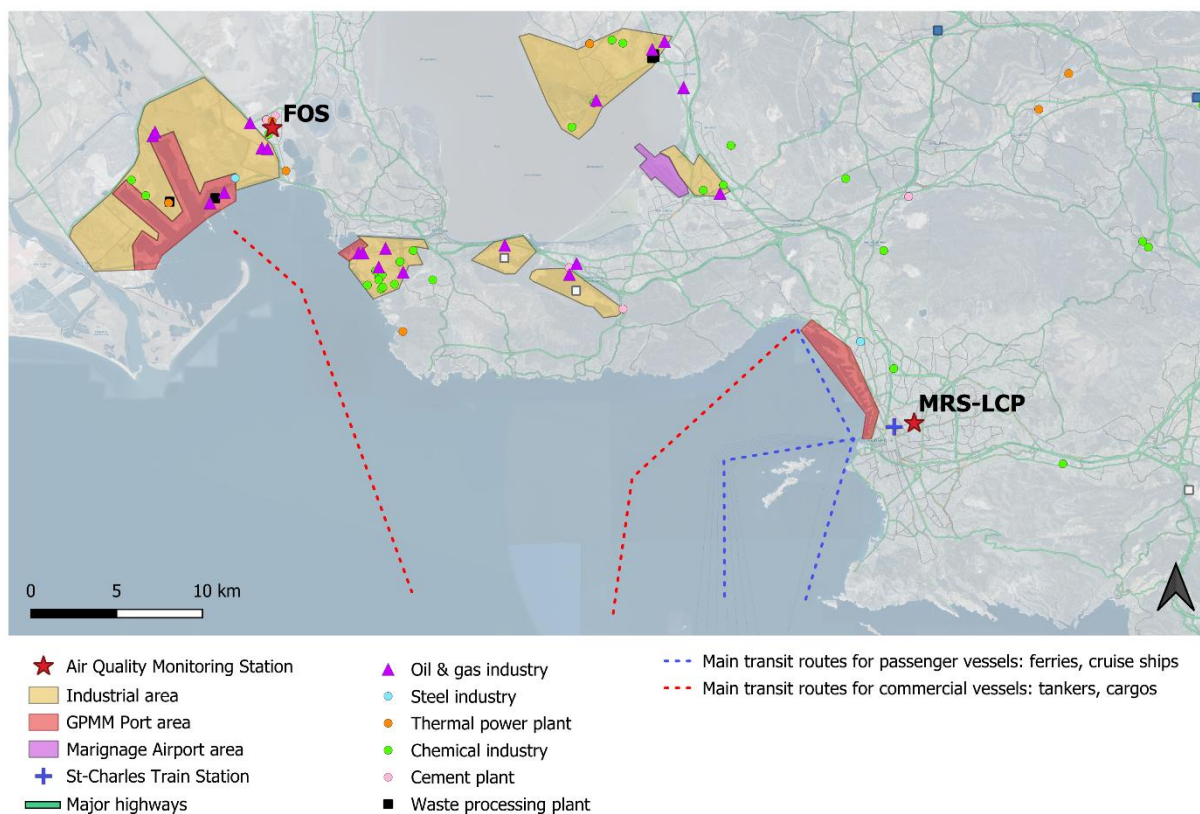


65 and contributions, we apply Rolling Positive Matrix Factorization (Rolling PMF), a dynamic source apportionment approach recently introduced by Canonaco et al. (2021). This method improves upon conventional static PMF by capturing short-term seasonal variations in factor profiles. Although Rolling PMF has been widely used for AMS/ACSM datasets (Heikkinen et al., 2021; Tobler et al., 2021; Chen et al., 2021, 2022a, 2022b; Lin et al., 2022; Via et al., 2022; Chazeau et al., 2022; Chebaicheb et al., 2023; Lei et al., 2025), its application to Xact data remains limited (Manousakas et al., 2025) and no application of Rolling PMF methodology upon 1 year-long Xact data has been reported yet. This is particularly important because several non-metal elements measured by the Xact (e.g., S, Se, Cl, Br) can undergo rapid atmospheric transformations, which static PMF approaches may fail to capture.

2 Instrument & Methods

2.1 Dual-Site Description

75 The Marseille-Fos basin is a semi-enclosed coastal basin in the northwestern Mediterranean, covering nearly 2500 km² and including the Gulf of Fos-sur-Mer and the Bay of Marseille, the second most populated city in France. The region experiences intensive anthropogenic pressure due to major industrial, urban, and maritime activities (Fig. 1). The Berre Pond industrial area is one of the largest in France, encompassing steel manufacturing plants, oil refineries, petrochemical facilities, cement factories, and stone quarries, and the Fos-sur-Mer incinerator. Additionally, a major thermal power plant, 80 the Gardanne facility, is located 20 km north-east of Marseille's city centre (Fig. 1). In parallel, the Grand Port Maritime de Marseille (GPMM), the second-largest port in France, extends from Fos-sur-Mer to the northern part of Marseille. In 2023, the GPMM processed over 72 million tonnes of goods and welcomed more than 4 million cruise passengers (<https://www.marseille-port.fr>). It comprises the Fos industrial harbour (between Port-Saint-Louis and Fos-sur-Mer) and the Port-de-Bouc terminal at the entrance of the Berre Channel. Together, these facilities delimit the Gulf of Fos, forming the 85 largest industrial-port complex in France. On the other side of the basin, previous studies have demonstrated that maritime traffic in the Bay of Marseille, including emissions from vessels at berth, contributes significantly to urban air pollution levels (Chazeau et al., 2021; Le Berre et al., 2025). Additionally, Marseille is characterized by intense vehicular activity as the city hosts the second largest car fleet in France (Bilan Annuel des Transports 2023, <https://www.statistiques.developpement-durable.gouv.fr/>).



90

Figure 1: Map of the Marseille–Fos basin. Locations of industrial plants were obtained from the SEVESO and IREP databases (<https://data.ampmetropole.fr/>). Main ship transit routes were derived from MarineTraffic (<https://www.marinetraffic.com/>). Major highways were sourced from Google Traffic (©Google). Background map layers were provided by Carto Positron and Bing Satellite. The map was produced using QGIS 3.34.

95 The combination of such diverse anthropogenic activities generates a complex mixture of primary pollutants, which undergo chemical transformation and are transported across the Marseille-Fos basin. The region is characterized by high solar radiation during summer, promoting photochemical activity, including ozone formation and secondary organic aerosol (SOA) production (El Haddad et al., 2013; Chazeau et al., 2021). Prevailing wind regimes in the Marseille-Fos basin are dominated by the Mistral and thermal breezes, both playing a major role in pollutant transport. The Mistral, a synoptic northwesterly wind (270°-360°) channeled through the Rhône Valley, would be expected to affect both sites similarly; however, it was reported 54 % of the time at Fos-sur-Mer and 35 % at Marseille in 2023, likely reflecting local shielding effects from surrounding hills and vegetation. Thermal breezes were observed approximately 40% of the time in the Marseille-Fos basin. These are characterized by nocturnal land breezes (5°-90°) and daytime sea breezes (210°-270° in Marseille; 120°-240° in Fos-sur-Mer). In addition, the region is occasionally impacted by strong southeasterly Sirocco winds, which transport Saharan dust across the Mediterranean (Flaounas et al., 2009). In 2023, six dust episodes, lasting

100

105



from 1 to 4 days, were recorded. The basin's complex topography further modulates atmospheric transport. Marseille is also bordered by mountainous terrain, with the Massif de l'Étoile to the north (778 m a.s.l.) and the Calanques massifs to the south (646 m a.s.l.). The combination of complex terrain and variable meteorological conditions results in substantial variability in the Boundary Layer Height (BLH), ranging from over 1000 m during summer Mistral events to below 500 m under wintertime thermal breeze conditions (Riandet et al., 2023), thus affecting aerosol dispersion and dilution.

To investigate the atmospheric composition in this complex environment, data from two air quality monitoring supersites were used, both operated by the Laboratory of Environmental Chemistry (LCE) and AtmoSud (<https://www.atmosud.org>). The first one, the Marseille-Longchamp Observatory supersite (MRS-LCP), is located in the center of Marseille, in Longchamp Park near the Marseille Observatory (43°18'18.84" N, 5°23'40.89" E; 71 m a.s.l.). Continuously operating for nearly two decades, this station is classified as an urban background site according to European Environment Agency criteria (Larssen et al., 1999). Positioned approximately 3 km inland from the Mediterranean coastline and within the city center, it is representative of typical coastal urban air quality conditions. MRS-LCP has been featured in multiple studies (El Haddad et al., 2011; Salameh et al., 2018; Chazeau et al., 2021; Camman et al., 2024) and has been recently selected as a French urban super sites for the new EU regulation. The second site, the Fos-Carabins Monitoring Station (FOS, 43°27'32.092" N ; 4°56'4.412" E ; 5 m a.s.l.), is located in the residential area of Fos Les Carabins but is classified as periurban site under industrial influence due to its proximity to the port-industrial complex of Fos-sur-Mer and its exposure to emissions from surrounding industrial facilities, including the ones of Fos-sur-Mer (< 1km southwest), and Port-de-Bouc (approximately 10 km southeast, Fig. 1). Like MRS-LCP, the FOS station is located approximately 3 km from the coastline. Despite being 40 km apart, meteorological conditions enable the transport of aerosol between both sites from several emissions sources. Specifically, sea-breeze events frequently carry industrial plumes inland toward Marseille (Puygrenier et al., 2005; El Haddad et al., 2013), while low Mistral flows may facilitate downwind transport of pollutants from the Fos-sur-Mer industrial area toward the urban center. Therefore, both monitoring sites are strategically positioned to assess intra-basin transport and the interplay between urban and industrial sources.

2.2 Sampling and Instrumentation

Submicronic aerosols were continuously sampled from January 1st, 2023, to December 31st, 2023, as part of the SHIPAIR ("SHIPPING emission's contribution to AIRpollution in urban harbour area") campaign (<https://anr.fr/Project-ANR-21-CE22-0015>) at both sites. Each sampling station was equipped with a range of analytical instruments for aerosol and gases monitoring, as detailed in Table 1.

135

Instrument	Species	Fraction	Temporal Resolution	Technology	MRS-LCP	FOS
------------	---------	----------	---------------------	------------	---------	-----



Xact 625i Cooper Environmental	Trace elements	PM ₁	1h	X-Ray fluorescence (XRF)	X	X
Tof-ACSM Aerodyne Research	Non-refractory aerosol	PM ₁	10 min	Electron Ionisation and Time-Of-Flight Mass Spectrometry	X	
AE33 Aerosol Magee Scientific	Black carbon	PM _{2.5}	1 min	Spectroscopy	X	X
SMPS 3031 TSI	Particles number and Granulometry	15 nm - 723 nm	5 min	Electric field isolation and optical counting	X	
FIDAS 200 PALAS	Mass concentration	180nm – 20µm	15 min	Optical light scattering	X	
M200E Teledyne API	NO _x	Gas	15 min	Chemiluminescence	X	
M100 E Teledyne API	SO ₂	Gas	15 min	UV Fluorescence	X	X
Serinus 10 Ecotech	O ₃	Gas	15 min	UV Spectroscopy	X	
VOC72M Envea	BTEX, cyclohexane, Cl-Volatile Organic Compounds (Cl- VOCs): 1,2- dichloroethyl, trichloroethyl, tetrachloroethyl	Gas	1h	Gas Chromatography and photo-ionisation detector		X

Table 1: Overview of the instruments deployed during the field campaign at MRS-LCP and FOS monitoring stations.

At both sites, aerosols for elemental analysis were continuously and automatically sampled using a PM₁₀ inlet (Tisch environmental, Cleves, OH, USA) coupled with a PM₁ impactor, operating at a flow rate of 16.7 L·min⁻¹. Airborne elements
 140 were quantified by energy-dispersive X-ray fluorescence (ED-XRF) using the Xact 625i analyzer (Cooper Environmental Services, Edgartown, MA, USA). Briefly, Particulate matter (PM) was collected onto a Teflon filter tape (PTFE membrane, 2µm thickness, Cooper Environmental Services). Then, incident X-rays from the tube excite the inner-shell electrons of the



sampled particles, generating element-specific secondary X-rays detected by a solid-state fluorescence detector. This enables both identification and quantification of elements (Currie, 1977; Furger et al., 2017).

145 The instrument is designed to simultaneously quantify up to 45 elements, from Al to Bi (Xact 625i Manual, Cooper Environmental Services, Table S1). For MRS-LCP and FOS, 33 elements (Fig. S1) and 27 elements (Fig. S2), respectively, were individually calibrated using pure element standards provided by the manufacturer.

The Xact 625i enables online sampling and analysis of airborne elements over extended monitoring periods (several months) at high temporal resolution. The sampling and analysis cycle ranges from 5 to 240 minutes. However, to allow for reasonable

150 Minimum Detection Limits (MDLs), a 60-minute sampling and analysis cycle was selected for this campaign. Nevertheless, there are some limitations to the use of the instrument. First, MDLs reported for the Xact 625i are generally higher than those obtained with offline elemental aerosol analysis methodologies (XRF or inductively coupled plasma mass spectrometry, ICP-MS) (Tremper et al., 2018; Cadeo et al., 2025). Moreover, due to the self-absorption effect for low energy X-rays emitted by lighter elements ($Z < 15$) (Formenti et al., 2010), the Xact 625i cannot detect elements such as Na or Mg,

155 while other elements such as Al or Si show higher MDLs (Table S1). Comparatively, synchrotron radiation-induced (SR) XRF and ICP-MS techniques allow the detection of a larger range of elements (SR-XRF: $Z > 11$; ICP-MS: Na, Mg) (Visser et al., 2015a; Furger et al., 2017). The lack of quantitative assessment of Na and Mg causes strong limitations for coastal sites like ours where these elements provide key information on marine aerosols, (e.g. fresh and aged sea salt, Pey et al., 2013a).

160 Other ancillary continuous monitoring of regulated pollutants were conducted exclusively at the MRS-LCP. Mass concentrations of PM_{10} , $PM_{2.5}$ and PM_{10} were measured using a FIDAS 200 optical particle counter (PALAS, Germany). Data were recorded at 15-minute resolution throughout the entire measurement period. In parallel, NO_x (M200E, Teledyne API, California, USA) and SO_2 (M100E, Teledyne API, California, USA) were also measured continuously with the same 15-minute time resolution, with additional SO_2 monitoring using the same technique at FOS. Non-refractory (NR) PM_{10} were

165 sampled using Time-of-Flight Aerosol Chemical Speciation Monitor (ToF-ACSM, Aerodyne Research Inc., USA; Fröhlich et al., 2013) for the determination of organic aerosol (OA), NH_4^+ , NO_3^- , SO_4^{2-} , and Cl^- concentrations. During the whole year, data were acquired and compiled at 10-minute time resolution through Igor-DAQ software, Tofware (Tofwerk, Thun, Switzerland). Particle number size distributions (PNSD) in the submicron range were measured at MRS-LCP only, using Scanning Mobility Particle Sizers (SMPS) with an Ultrafine Particle Counter model 3938 (TSI Inc., Minnesota, USA, CPC

170 3752, classifier 3082) providing particle counts from 15 to 723 nm every 5 min in 55 size bins.

Black carbon (BC) analysis was carried out at both sites with aethalometer AE33 (Magee Scientific, CA, USA) operated with a $PM_{2.5}$ inlet. The dual-spot sampling method (Drinovec et al., 2015) was used to correct for filter-loading artifacts (Lack et al., 2014). BC was further apportioned into BC liquid fuel (BC_{LF}) and BC solid fuel (BC_{SF}) components using the Aethalometer model (Sandradewi et al., 2008b; Chazeau et al., 2021).



175 Volatile organic compounds (VOCs) including cyclohexane, 1,2-dichloroethane, trichloroethene, tetrachloroethene, and BTEX (benzene, toluene, ethylbenzene, and o-, m-, and p-xylenes) were measured hourly at the FOS site using a VOC72M gas chromatograph equipped with a photo-ionisation detector (Envea, France).

Meteorological data, including temperature, wind direction and wind speed, were recorded at both sites with an Ultrasonic 3D anemometer USA-1 (METEK, Germany). Shortwave radiation and boundary layer height (BLH) for the Marseille-Fos
180 area during 2023 were retrieved from the Open-Meteo meteorological database (<https://open-meteo.com/>). Both stations were connected to automated data platforms (e.g. the eSAM system, Envea), enabling daily automated quality control and continuous data recording. Instruments and annual datasets visualization from both stations is accessible through the HERMES platform (HERald of the MEasurement Stations, <https://hermes-aq.com/>).

185 **2.3 Source Apportionment methodology**

Detailed information on the source apportionment methodology is provided in Supplement S1: PMF methodology. Briefly, Positive Matrix Factorization (PMF) is a bilinear receptor model that decomposes a chemical matrix into factor time series and profiles, which can then be interpreted as emission sources (Paatero & Tapper, 1994). Unlike Principal Component Analysis (PCA) or Chemical Mass balance (CMB), PMF imposes non-negativity and requires little a priori information,
190 making it particularly suited for environmental applications. The model iteratively minimises the weighted residuals (Q), with “robust” mode applied to downweight outliers (Paatero, 1997). Rotational ambiguity is addressed using the ME-2 solver, where the a-value approach constrains selected factors within predefined variability ranges (Paatero & Hopke, 2009). Finally, the bootstrap resampling method (Efron, 1979; Ulbrich et al., 2009) provides statistical uncertainty estimates by testing the stability of factors across perturbed datasets.

195 Yet, a stable statistical solution does not guarantee environmental meaning. For long-term datasets, covering several months to a full year, PMF factor profiles may exhibit seasonal variability that is not captured by the static PMF method. To address this, Parworth et al. (2015) introduced the Rolling PMF approach, which applies PMF in a rolling window to capture temporal variability in factors. This method allows for the identification of short-term source behaviour that would otherwise be averaged out in static analyses. In this study, both static and rolling PMF analyses were applied to hourly trace element
200 data, at both the urban MRS-LCP and industrial FOS sites. Analyses were conducted using the SoFi Pro (Source Finder) toolkit (Datalystica Ltd., Villigen, Switzerland, Canonaco et al., 2013; 2021), an Igor Pro based program (WaveMetrics, Inc., Portland, OR, USA).

PMF results from both static and rolling approaches were compared in terms of their ability to capture temporal variability of sources, by analyzing the dissimilarity of the factor profiles using Pearson Distance and Standardized Identity Distance (PD-
205 SID) analysis (S2: PD-SID; Belis et al., 2015; Pernigotti & Belis, 2018). While PD-SID has been widely used to assess factor homogeneity across multiple sites (Weber et al., 2019; Borlaza et al., 2021; Manousakas et al., 2022; Liu et al., 2025), few studies have reported its use for evaluating factor homogeneity at a single site (Ngoc Thuy et al., 2025). Additionally,



cosine similarity, commonly employed to calculate correlations between mass spectra (Stein & Scott, 1994; Ulbrich et al., 2009), was adapted to elemental factor compositions (Cosine Distance, CD, S3: Cosine Distance) to assess the variability of
210 PMF factor profiles between static and rolling approaches.

3 Rolling Positive Matrix Factorization Setup

3.1 Data Validation & Xact PMF Matrix Preparation

Over the year, airborne elements measured by the Xact contributed approximately 8% to the reconstructed PM_i mass at MRS-LCP (S4: PM_i Mass Reconstruction at MRS-LCP, Fig. S3 & S4). A total of 18 elements were selected for PMF
215 analysis at both sites (Fig. S1 & S2): S, Cl, K, Ca, Ti, V, Cr, Mn, Fe, Ni, Cu, Zn, As, Se, Br, Cd, Pb, along with Pd (specific to MRS-LCP) and Rb (specific to FOS). Element selection was based on the proportion of data below MDLs (BDL), using a threshold of 88 %, which is close to the 90 % BDL level applied in a previous Xact-PMF study at MRS-LCP (Camman et al., 2024). This threshold is higher than the 70 % BDL criterion adopted in another Xact-PMF study (Manousakas et al., 2022), in order to retain short but intense industrial events driven by anthropogenic markers such as Pb (82 % BDL at MRS-
220 LCP). Some exceptions were made to maintain a consistent set of elements across both sites. Specifically, Mn (90.8% BDL), Cd (92.7% BDL), and Cr (94.6% BDL) at MRS-LCP were kept to match the elements used at FOS for homogeneous PMF analysis. Another exception was made for Rb at FOS (96.3% BDL), which proved to be a relevant tracer for biomass burning emissions during winter (Massimi et al., 2020). However, for the majority of elements, the BDL fraction was below 60% (Tables S2 & S3).

225 The input matrix for the PMF analysis was constructed following the methodology proposed by Polissar et al. (1998b): values below the MDL were replaced with MDL/2, and their associated uncertainties were set to 5/6 of the MDL. For values above the MDL, the error was computed as the square root of the quadratic sum of the MDL and the estimated measurement uncertainty from the Xact instrument (Reff et al., 2007; Camman et al., 2024). In addition, a cell-wise downweighting approach was applied to data with a signal-to-noise ratio (SNR) below 2, as proposed by Visser et al. (2015b). For these low-
230 SNR values, the associated uncertainty was replaced with a penalized error defined by the function $2/\text{SNR}_{ij}$. Short-lived events (1 h to 2-3 days), such as Sirocco episodes, construction activities, or fireworks, were excluded from the dataset. These episodes disrupted factor analysis (e.g., Dust, Steel Industry) but could not be attributed to a specific factor due to their chemical similarity with other sources (e.g., Saharan dust and local dust, fireworks and biomass burning). The methodology for their identification and exclusion is described in S5: Data correction (Fig. S5).

235 The ToF-ACSM data at MRS-LCP were also analyzed for the same period using rolling PMF following the ACSM Standard Operating Procedure established within the COLOSSAL project (COLOSSAL, 2021), as detailed in Chen et al. (2022) and Chazeau et al., (2022). A total of five organic aerosol factors were resolved for the year 2023 (Fig. S6). Among them, the Biomass Burning Organic Aerosol (BBOA), displayed marked seasonal variability, with no contribution observed between May and September. The Hydrocarbon-like Organic Aerosol (HOA) factor was predominantly associated with traffic



240 emissions, while the Cooking Organic Aerosol (COA) factor originated from food preparation activities. Two additional factors were attributed to long-range transported secondary organic aerosols: More Oxidized Oxygenated Organic Aerosol (MOOOA) and Less Oxidized Oxygenated Organic Aerosol (LOOOA). These results are consistent with previous studies at the MRS-LCP site (Chazeau et al., 2022) and will be used to support interpretations of elemental concentration variations.

245 3.2 Static PMF analysis for Airborne Elements

As limited information was available on Xact PMF factors in the region (Camman et al., 2024), static PMF analyses were first performed to define reasonable PMF solutions. Each site was treated independently to ensure site-specific interpretation. PMF solutions for the full 2023 dataset (YEAR), ranging from 5 to 12 factors, were evaluated to identify the most meaningful configuration for each site. Statistical diagnostics (Q/Q_{exp} and unexplained variation, UEV) suggested optimal solutions of 9 factors for MRS-LCP and 8 for FOS (Fig. S7). However, examination of factor time series, daily trends, chemical composition, and geographical origins indicated that the most environmentally interpretable solutions were obtained with 8 factors at MRS-LCP and 9 at FOS (Table S4).

To investigate seasonal variability in source contributions, each PMF dataset was divided into 4 seasons: JF_D: January, February, December, MAM: March, April, May, JJA: June, July, August, and SON: September, October, November. Unconstrained preliminary runs revealed that some factors, such as the Cl-rich (4.2.7) and the Shipping (4.2.1), exhibited strong seasonality at both sites and could not be clearly identified in some periods unless constrained. For instance, the Shipping factor was not retrieved during winter at both site (Tables S5 & S6), probably due to reduced sea breeze advection of shipping plumes (Chazeau et al., 2021). Similarly, during JJA the Cl-rich factor was partly mixed with Dust in unconstrained runs (Tables S5 & S6). Although Dust may contain some residual Cl (Visser et al., 2015b), this is not consistent with the other seasons PMF results. To address these seasonal inconsistencies, following an approach similar to Chazeau et al. (2022), reference factor profiles were extracted from PMF solutions with a higher number of factors. An 11-factor solution enabled the identification of the Shipping factor during JF_D and a distinct Cl-rich factor during JJA. These reference profiles were subsequently used to constrain the Shipping and Cl-rich factors during JF_D and JJA, respectively, using the a-value approach, with random a-values ranging from 0 to 0.5 in steps of 0.05 for the static PMF analysis and bootstrap runs.

Unlike the OA rolling PMF, where BBOA is resolved only from September to May, the Xact rolling PMF retained a Biomass Burning factor throughout the year. This choice reflects the expectation of year-round biomass burning emissions (e.g., wildfires, crop burning, barbecue) and avoids unrealistic redistribution of K into other factors. The relevance of this approach is supported by the year-round presence of BC_{SF} and its consistent correlation with the final Biomass Burning factor (4.2.2).

To assess the statistical uncertainty of the factor profiles, each seasonal PMF solution was then bootstrapped 100 times. To retain only environmentally meaningful runs, a set of custom criteria was applied to the bootstrap outputs. These criteria,



based on the tracer element apportioned to each factor, proved more effective in filtering out "mixed" or inconsistent solutions. The complete list of criteria and associated thresholds for each PMF solution, as well as the percentage of retained
275 bootstrap runs, are provided in Supplements (Tables S7 & S8, respectively).

3.3 Rolling PMF Parametrization

To capture fine temporal variability of sources, rolling PMF was applied at both sites using the same dataset as for the static PMF. As preliminary static PMF solutions showed high similarity for common factors at both sites (3.2), rolling PMF
280 parameter optimization was performed only for the MRS-LCP dataset. The resulting optimal settings were then applied to the FOS dataset.

Canonaco et al. (2021) proposed a method to determine the best rolling PMF parameters. Rolling PMF implemented in SoFi allows for adjustment of several key parameters, including rolling window size, number of PMF repeats per window, and the number of days by which the window is shifted, in addition to static PMF options such as factor constraints and a-value
285 configuration. Similar to the approach used in Canonaco et al. (2021), we developed a method based on statistical indicators, namely Q/Q_{exp} , percentage of unselected PMF runs and total UEV, to select optimal rolling PMF settings (rolling window size, maximum a-value, and PMF repeats per window). Previous Rolling PMF study with ACSM datasets (Canonaco et al., 2021; Chen et al., 2021) used the percentage of non-modeled data points to determine the minimum number of PMF repeats per window required to ensure 0% non-modeled points. However, this criterion was not applicable here, as nearly all
290 modeled points met the selection criteria, even with a low number of repeats, likely due to differences in the selection criteria applied in both studies. We used instead the percentage of unselected runs. Window sizes of 7, 14, 21, and 28 days were tested, with the rolling window shifted by 1 day over the entire dataset. Maximal a-values of 0.2, 0.4, and 0.6 were explored, and PMF repeats per window were set to 1, 5, 10, and 50 successively. As testing all combinations of the three parameters ($4 \times 3 \times 4 = 48$ rolling PMF tests) would require many days of computation on a modern multicore PC, each rolling PMF run
295 taking approximately 6 hours, we adopted a base-case configuration (rolling window size = 14 days, a-value = 0.4, PMF repeats per window = 10). In each Rolling PMF test run, only one parameter was modified while the other two were held constant (base-case values), following the approach of Canonaco et al. (2021).

The window size is a critical parameter in rolling PMF, as it determines the ability to resolve short-term temporal variability of evolving factor profiles and to assess the lifetime of aerosol sources. Previous studies on organic aerosol PMF have
300 commonly selected 14-days windows (Parworth et al., 2015; Canonaco et al., 2021; Chazeau et al., 2022; Chen et al., 2022; Via et al., 2022). In this study, statistical analysis (mean Q/Q_{exp} , percentage of unselected runs, and total UEV) indicated that both 14-days and 21-days windows were acceptable (Fig. S8). However, some geochemical considerations supported the use of a 21-days window. First, Xact provides direct elemental quantification; consequently, redox changes without a phase change (e.g., $\text{SO}_2(\text{g})/\text{SO}_4^{2-}(\text{p})$) are not observable, whereas the ACSM captures organic aerosol oxidation through changes in
305 m/z signatures. As a result, metallic aerosol signals measured by Xact are expected to exhibit longer apparent atmospheric



residence times than organic aerosol components measured by the ACSM. Furthermore, the particularly dry conditions in 2023 (Météo-France, 2023) limited wet deposition, and metals, primarily found in fine particles, typically exhibit longer atmospheric lifetimes (Roy et al., 2019). Together, these factors justified selecting a 21-day window for the final analyses. As shown earlier (3.2), the Cl-rich and Shipping factors showed strong seasonality and therefore required constraints. Unlike
310 the seasonal static approach, rolling PMF operates on the full annual dataset; reference profiles were thus selected from the periods in which each factor was most robustly resolved (eg. summer for Shipping and winter for Cl-rich, Tables S5 & S6). Constraints were applied using randomly selected a-values, varying from 0 up to a maximum a-value in increments of 0.05. The maximum a-value was tested at 0.2, 0.4, and 0.6. This narrower range, compared with that explored by Canonaco et al. (2021), was chosen to avoid over-constraining the factors and to prevent unnecessary computational load. Sensitivity tests
315 showed that maximal a-value had minimal influence on the key statistical indicators (Fig. S8), and a maximum a-value of 0.4 was ultimately selected, consistent with the recommendations of Canonaco et al. (2021).

To determine the minimal number of PMF repeats per window, we evaluated both the percentage of unselected runs and the minimum number of PMF repeats per modeled day while varying the total repeats per window, with bootstrapping enabled. The percentage of unselected runs showed no significant variation with the number of PMF repeats per rolling window (Fig.
320 S8). While this metric provides a general indication of the statistical robustness of the rolling PMF parametrization, it does not reflect the temporal variability in the model's ability to resolve source apportionment at specific times of the year. To better assess this aspect, we evaluated the number of PMF repeats per modeled day in the final solution (Table S9). A minimum threshold of 10 PMF repeats per modeled day was adopted, leading to a requirement of at least 50 PMF repeats per window. Finally, the detailed study of several Rolling PMF solutions at MRS-LCP showed best environmental accuracy and
325 statistical stability for 21 days rolling window length, 1-day delay and 50 repetitions per window with maximal a-value set to 0.4.

PMF factors at both sites were extracted using the same selection criteria as in the static analysis (3.2, Table S7), with additional conditions to improve factor classification. Specifically, the selected factor's score had to exceed that of the second-highest factor to avoid potential factor mixing, and each criterion score had to account for at least 30% of its specific
330 tracer (≥ 0.3). This additional condition was necessary to ensure a consistent classification of factors, especially given the wider variability in criterion scores allowed by the rolling approach (Fig. S9 & S10). Notably, while this variability reflects the challenges of applying selection criteria across the full annual dataset, it also highlights the strength of the rolling PMF method in capturing the temporal variability in factor composition.

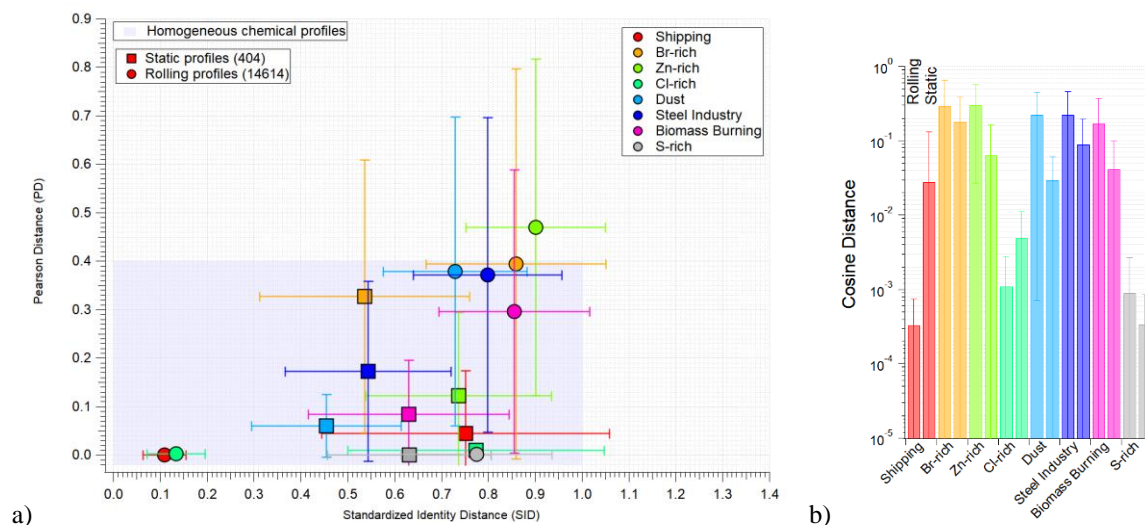


335 4 Results & Discussions

4.1 Comparative analysis: static vs rolling PMF approach

To compare factor profiles obtained from static and rolling PMF approaches, an extended analysis was performed for the eight factors resolved at MRS-LCP using both methods (static PMF for YEAR, JF_D, MAM, JJA, and SON, and rolling PMF). First, comparing elements apportionment for each method, shows that the rolling PMF leads to lower UEV for most elements (Fig. S11). Furthermore, most factors, except the S-rich factor, exhibit higher S enrichment in the rolling solution, concomitant with a reduced S contribution in the S-rich factor itself (Fig. S12). This redistribution results in increased mass contributions for several factors. Such differences are particularly relevant given the wide range of potential sources contributing to secondary sulfate formation (e.g., various industrial activities, shipping), while the accurate attribution of the sulfate origins remains challenging (Chazeau et al., 2021; Su et al., 2025).

To further assess intra-variability of factor profiles resolved by static and rolling PMF, all factor profiles obtained at MRS-LCP were extracted from the bootstrapped PMF outputs. This included 404 profiles from the static PMF analysis and 14,614 profiles from the rolling PMF analysis. Pairwise PD-SID and CD (2.3) were then calculated for each factor and each method (8 factors \times 2 methods). For each factor, this resulted in $n(n-1)/2$ profile comparisons, where n is the number of profiles obtained with a given PMF approach. Both PD-SID (Fig. 2a) and CD analyses (Fig. 2b) indicate larger variability in factor profiles resolved by the dynamic approach compared to the static one, for both major (PD) and trace elements (SID). This trend was observed for all factors except the constrained ones (Shipping, Cl-rich), highlighting the critical importance of reference profile selection when applying constraints (3.2, 3.3). The S-rich factor showed relatively low PD enhancement and CD under the rolling approach, consistent with the dominance of sulfur in the elemental mass and the persistence of large-scale sulfate formation from photooxidation in the basin (4.2.9). By contrast, the Zn-rich factor exhibited PD-SID values above the range of homogeneous chemical profiles, suggesting possible contributions from multiple sources, similar to what have been stated in 4.2.6.



360 **Figure 2:** a) PD-SID similarity plot of the factors obtained with the static (square) versus dynamic (round) PMF approaches. The blue shaded area shows the limit of the homogeneous chemical profile. For each point, round and square markers indicate the average distance from the $n(n-1)/2$ profile comparisons, and the error bars represent the standard deviation when comparing all pairs of factors for the 404 static profiles vs. the 14614 dynamic profiles. b) Cosine Distance similarity plot of the factors from both PMF approaches (rolling on the left, static on the right for each bar).

To assess the temporal variability of factor composition within the rolling PMF approach, PMF runs were attributed to individual days of the dataset. Using a 21-days window, a 1-day shift, and 50 PMF repeats per window, each day was represented by approximately 50 selected PMF runs (after applying the selection criteria; 3.3), corresponding to all rolling windows including that day. For each factor, daily rolling PMF profiles were compared to the corresponding static (YEAR) profiles by calculating the CD (Fig. S13). The mean and standard deviation of these metrics were then derived for each factor. In organic aerosol PMF studies, CD values above ~ 0.15 ($\theta > 30^\circ$) are generally considered indicative of weak similarity (Bougiatioti et al., 2014). The daily CD between rolling and static factor profiles shows minimal variation for the S-rich factor and for the constrained Shipping and Cl-rich factors, consistent with previous results. In contrast, the Br-rich, Zn-rich, Dust, Steel Industry, and Biomass Burning factors exhibit pronounced increases in CD (> 0.15) during specific periods of the year, indicating substantial temporal variability in source chemical composition that is effectively captured by the rolling PMF approach.

Detailed analyses of the daily CD for the Biomass Burning factor (Fig. S14) reveal large deviations during summer, associated with enhanced sulfur enrichment. This behavior is consistent with previously reported increases in S/K ratios with the aging of biomass burning emissions (Viana et al., 2013). These results support the interpretation that Biomass Burning is mainly driven by fresh and local residential heating during winter, whereas summertime rolling profiles reflect distant sources (e.g., wildfires, agricultural burning, barbecuing), combined with enhanced photochemical conversion of SO₂ to particulate sulfate under higher solar radiation. In contrast, the static PMF approach yields a Biomass Burning factor largely



380 dominated by wintertime residential solid-fuel combustion and is therefore unable to adequately represent summertime biomass burning emissions.

Overall, these results demonstrate the improved ability of the rolling PMF approach to capture seasonal variability and short-term changes in aerosol composition. However, further work is needed to fully understand submicron airborne elements sources in the region and to assess the geochemical relevance of short-lived rolling PMF profiles.

385 4.2 Interpretation of PMF factors

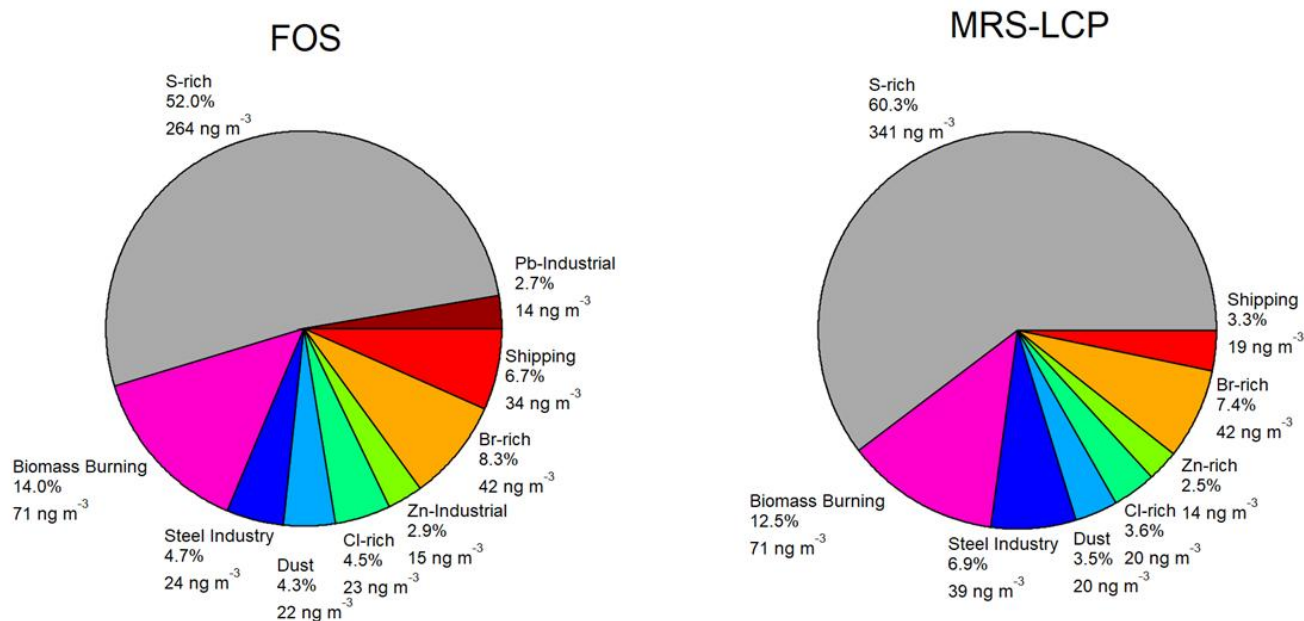
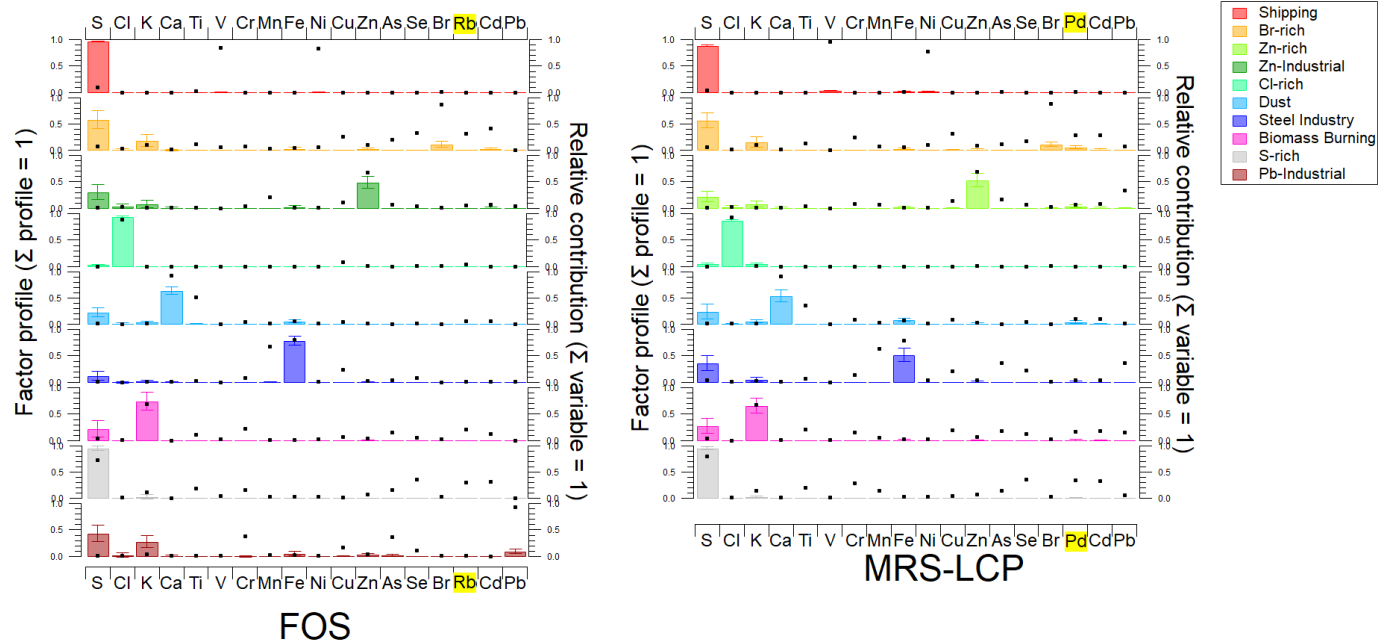


Figure 3: Pie chart showing the average mass contribution of Xact rolling PMF factors for FOS (left) and MRS-LCP (right).



390 **Figure 4: Final rolling PMF factors profile for FOS (left) and MRS-LCP (right). The colored bar plots represent factor profile contribution (left axis), while black markers indicate the relative contribution of each variable (right axis). The yellow-highlighted letters denote the two differing elements between both sites.**

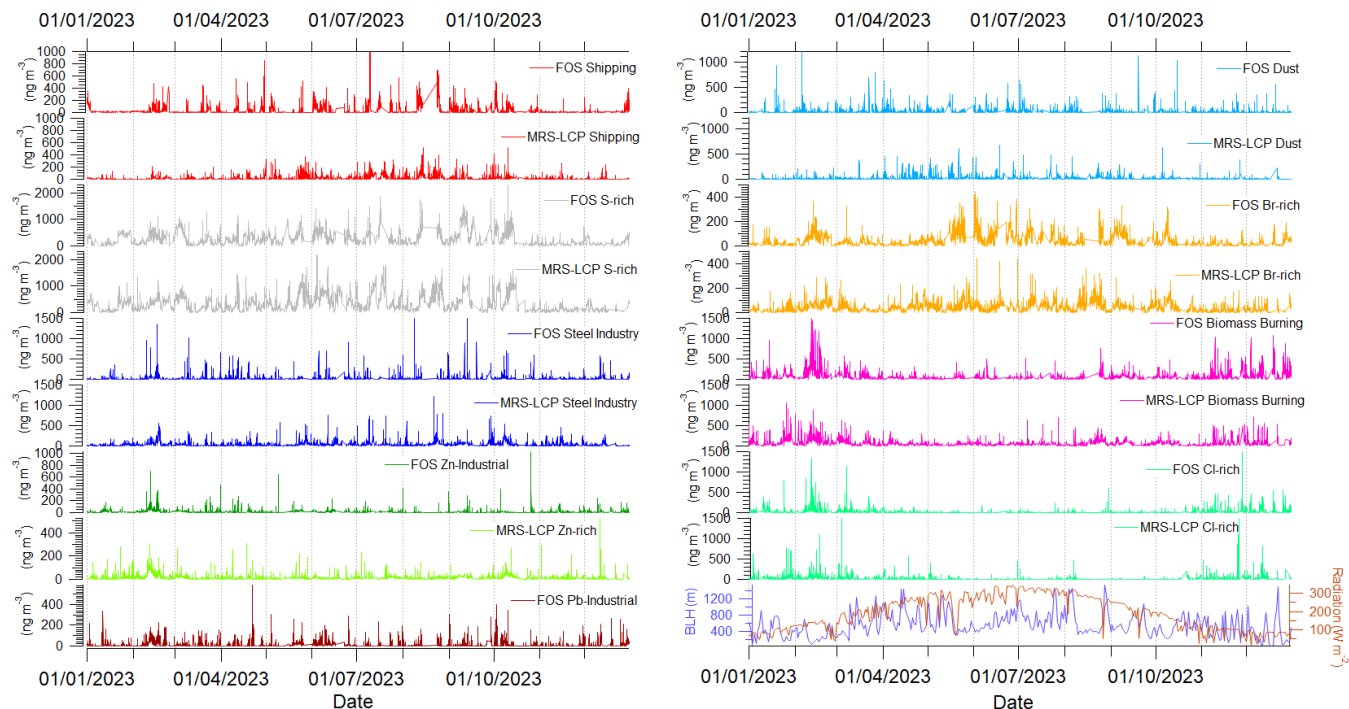
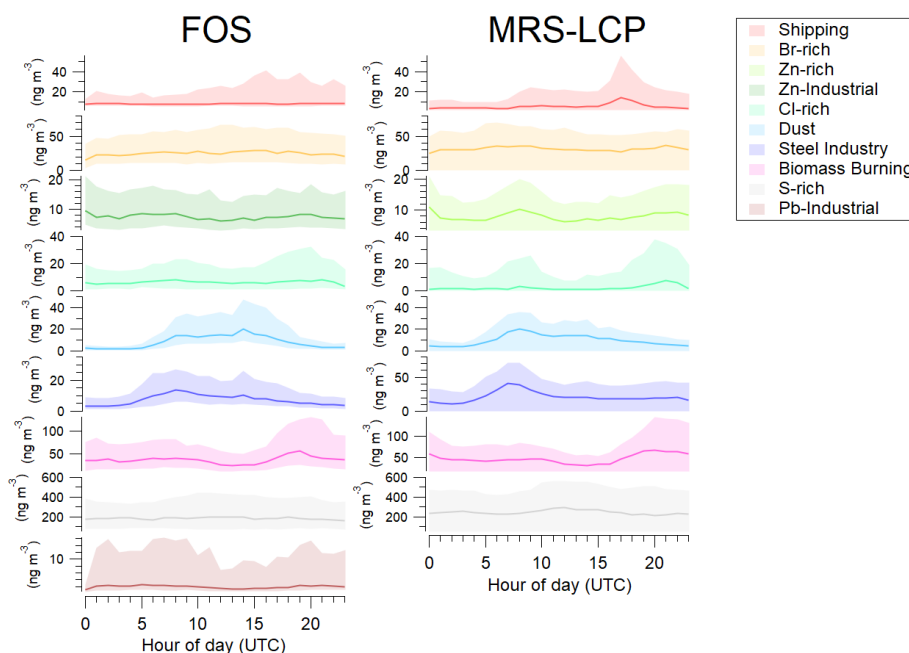




Figure 5: Factors times series for the final rolling PMF solution. Shortwave radiation and boundary layer height (BLH) for the Marseille-Fos basin area during the year 2023 were obtained from OpenMeteo (<https://open-meteo.com/>).



395

Figure 6: Diurnal patterns for FOS (left) and MRS-LCP (right). The colored lines represent the median diurnal evolution of each factor, the dashed lines indicate the mean diurnal evolution, and the light-colored areas show the interquartile range.

Rolling PMF analysis of PM₁ Xact data resolved nine factors at FOS and eight at MRS-LCP, including seven factors common to both sites (Figs. 3-6, S15-S18). These shared factors comprised S-rich, Br-rich, and Cl-rich factors associated with secondary aerosol formation, as well as Biomass Burning, Dust, Shipping, and Steel Industry. A Zn-rich factor was retrieved exclusively at MRS-LCP, while two additional industrial factors (i.e. Zn-Industrial and Pb-Industrial) were identified only at FOS. No distinct factor could be exclusively attributed to road transport emissions, as non-exhaust traffic-related metals are predominantly associated with coarse particles (Bukowiecki et al., 2009; Visser et al., 2015; Pant et al., 2017). Nevertheless, road transport may contribute to the Steel Industry and Zn-rich factors at MRS-LCP.

405 Secondary aerosols dominate the submicron elemental mass at both sites, with the S-rich factor accounting for more than half of the total PM₁ elemental mass. Biomass Burning represents the second largest contribution. The Dust factor contributes less than 5% at both sites, consistent with the predominance of crustal material in the coarse fraction (Pey et al., 2013a). Eventually, direct anthropogenic sources, including industrial factors (Steel Industry, Pb-Industrial, Zn-Industrial) and Shipping, each contribute less than 7% to the submicron elemental mass. Although these contributions to PM₁ mass are relatively small, their potential health impact may be significant. Specifically, shipping and industrial combustion processes are known to emit particles in the ultrafine size range (Jonsson et al., 2011; Riffault et al., 2015; Momenimovahed et al., 2021), which can penetrate deeply into the respiratory system and cause adverse health effects (Kreyling et al., 2006).

410



4.2.1 Shipping

415 At MRS-LCP, shipping emissions contributed approximately 6% to total PM₁ during summer 2018 (Camman et al., 2024).
In this study, Shipping emissions contributed to 6.7% and 3.3% of the total element mass of the PM₁ at FOS and MRS-LCP,
respectively (Fig. 3). At both sites, this factor was composed mainly of sulfur ($\geq 89\%$) and accounted for the majority of V
and Ni ($> 88\%$, Fig. 4), consistent with previous ED-XRF shipping emissions studies in Marseille (Le Berre et al., 2025) and
other coastal cities (Scerri et al., 2018; Fossum et al., 2024). Slight Fe enrichment at MRS-LCP (2%) may reflect ship
420 manoeuvring at berth (Le Berre et al., 2025).

Non-Parametric Wind Regression (NWR, Fig. S15 & S16) analyses further confirmed the maritime origin of the Shipping
factor. At both sites, shipping plumes were advected inland by daytime sea breeze, especially between May and October
(Fig. 6 & S19). Compared with MRS-LCP, the FOS site is less frequently influenced by sea-breeze circulation (Fig. S19),
likely intercepting shipping plumes more episodically and at a more aged stage. This is consistent with the higher sulfur
425 fraction observed at FOS ($96.8 \pm 0.6\%$) relative to MRS-LCP ($89.4 \pm 1.0\%$), reflecting enhanced secondary sulfate
formation during transport. The higher sulfur content also explains the larger average contribution of the Shipping factor at
FOS (34 ng m^{-3}) compared with MRS-LCP (19 ng m^{-3} ; Fig. 3). Moreover, the industrial Fos-sur-Mer harbour hosts many
tankers and cargo vessels awaiting port entry, as well as by tankers transiting through the Berre Channel (MarineTraffic,
<https://www.marinetraffic.com>). The longer residence time of these vessels in the Gulf of Fos-sur-Mer may further
430 contribute to the observed sulfur enrichment. Daily cycles further reflected port-specific activities (Fig. 6 & S20).
Marseille's port mainly serves passenger ships, with peak ship movements in the early morning (4:00-7:00 UTC) and late
afternoon (16:00-18:00 UTC), corresponding to two distinct peaks in the MRS-LCP shipping factor. In contrast, Fos-sur-Mer
GPM activity is dominated by cargo traffic, and FOS Shipping factor exhibited a flatter diurnal profile, with a slight
midday increase likely driven by sea breeze rise rather than increasing shipping traffic.

435 Consistent with recent IMO regulations and desulfurized fuel increased use (Yu et al., 2021; Fossum et al., 2024), V/Ni
ratios have decreased compared to pre-IMO values (1.2 ± 0.2 at MRS-LCP, 1.6 ± 0.3 at FOS vs. approximately 2 in summer
2018; Camman et al., 2024). Another consequence of IMO 2020 regulation is that SO₂, once a reliable tracer of shipping
emissions at MRS-LCP (Lu et al., 2006; Chazeau et al., 2022), no longer correlated with the shipping factor in 2023,
indicating effective reduction of SO₂ emissions.

440

4.2.2 Biomass Burning

The Biomass Burning factor was identified at both sites and contributed to more than 20% of the PM₁ elemental mass
concentration during winter (Fig. S21). It was primarily composed of K ($> 66\%$) and S ($> 22\%$), with trace elements such as
Rb (only at FOS, not calibrated in MRS-LCP), Cu, Cr, and As (Fig. 4).



445 Both sites exhibited typical daily cycles, with peak concentrations between 05:00-09:00 UTC and 19:00-23:00 UTC (Fig. 6),
reflecting increased night-time domestic heating. This trend closely aligns with the BBOA factor behavior reported at MRS-
LCP and in previous studies (Viana et al., 2013; Chazeau et al., 2022). NWR analyses showed a clear land-breeze influence
during winter, from the 5°-90° sector at both sites, consistent with biomass burning emissions transported by nocturnal land
breeze (Fig. S22-S23). At FOS, an additional contribution was observed from the southeast (125°-145°), possibly linked to
450 mixing with industrial combustion sources in the Port-de-Bouc area.

Significant correlations with other combustion-related markers confirmed the origin of the factor. At MRS-LCP, it was
correlated with BC_{SF} ($R = 0.78$) and BBOA ($R = 0.77$), and particle number concentrations in the 150-200 nm range ($R^2 =$
0.59, Fig. S24-S25), consistent with the size of biomass burning aerosols, which typically range from approximately 100 nm
(fresh) to 250 nm (aged) (Janhäll et al., 2010). At FOS, good correlations were observed with BC_{SF} ($R = 0.80$) and benzene
455 ($R = 0.69$) (Fig. S26). However, benzene is also emitted by industrial sources: NWR analyses indicate that, while winter
benzene shows a minor northeastern contribution, summer patterns are dominated by emissions from the Fos-sur-Mer and
Port-de-Bouc industrial areas (4.2.3, Fig. S27). This suggests that the Biomass Burning factor at FOS may include a partial
industrial combustion contribution.

Finally, factor at both sites exhibited traces of As, Cr, and Cu, which could result from the combustion of wood treated with
460 Chromium-Copper-Arsenate (CCA), (Solo-Gabriele et al., 2002; Wasson et al., 2005), a pesticide historically used for
timber preservation (Morais et al., 2021). Although CCA has been banned for commercial use in Europe since 2004, some
industrial applications remain permitted, and no specific guidance has been provided regarding the incineration of CCA-
treated wood (COMMISSION DIRECTIVE 2003/2/EC of 06/01/2003).

465 4.2.3 Pb-Industrial

This factor was exclusively identified at the FOS site. It represents 2.7% of the yearly average of the total elemental mass. It
was primarily composed of S (44%) and K (28%) and accounted for 93% of the total Pb mass (Fig. 4). It did not exhibit any
clear seasonal or diurnal variability (Fig. 6 & S21). Nevertheless, the NWR analysis revealed distinct contributions from the
235°-260° and 110°-150° sectors under relatively strong wind conditions, as well as a minor contribution from the 5°-90°
470 sector during winter only (Fig. S16 & S28). This latter contribution, typical of nocturnal land breeze transport, suggests a
possible influence from residential solid fuel combustion (4.2.2). The presence of Cr, Cu, and As traces, similar to the
Biomass Burning factor, further supports this potential mixing of biomass burning and industrial combustion. However, the
predominant southwesterly and southeasterly origins are indicative of industrial sources, likely associated with the Fos-sur-
Mer and Port-de-Bouc industrial complexes, respectively.

475 Fine airborne Pb has long been recognized as a marker of anthropogenic activities (Clements et al., 2014; Riffault et al.,
2015), and may originate from coal combustion (Alastuey et al., 2016; Rai et al., 2021), industrial processes (Moffet et al.,
2008; Manousakas et al., 2022), and waste incineration (Riffault et al., 2015). In the area, coal combustion is exclusively



associated with the steel industry in Fos-sur-Mer and therefore cannot account for the southeastern Pb contribution. A municipal waste incinerator located near the steel complex in Fos-sur-Mer, together with petrochemical and plastic-
480 processing facilities in the Port-de-Bouc industrial area, where open burning has been reported, likely account for the observed Pb, As, and Cd emissions (Valavanidis et al., 2008; Kumar et al., 2015).

Overall, the elemental composition, dominated by S, K, Pb, and As, and the observed wind directions suggest a combustion-related industrial source. Note that the Pb NWR at MRS-LCP indicates a dominant local and north-easterly origin, inconsistent with an industrial influence from the Berre Pond area (Fig. S29). Nevertheless, a partial contribution from the
485 west, confirms an influence of industrial Pb at MRS-LCP. This signal was largely captured within the Steel Industry factor but was not sufficient to resolve a distinct Pb-Industrial factor at this site (Fig. 4).

4.2.4 Steel Industry

A factor enriched in Fe (FOS: 80%, MRS-LCP: 51%) and S (FOS: 12%, MRS-LCP: 37%) was identified at both sites
490 accounting for the majority of Mn mass (>64%) (Fig. 4). This factor represents 4.7% and 6.9% of the total element mass of the PM₁ at FOS and MRS-LCP, respectively. At FOS, it clearly shows an origin from the 235°-260° sector aligning the steel industry in Fos-sur-Mer (Fig. S16). Furthermore, the presence of spikes in the time series (Fig. 5) strongly suggests an origin of intense and nearby industrial activity (Ledoux et al., 2006; Moreno et al., 2011a; Taiwo et al., 2014b; Almeida et al., 2015; Kfoury et al., 2015; Rai et al., 2020b; Rai et al., 2021). This is not surprising as the Berre Pond hosts one of the largest
495 steel plants in France, located at approximately 2km from the FOS sampling site (Fig. 1).

A previous study (Sylvestre et al., 2017) characterized fine particulate emissions downwind of this facility associated with high levels of Fe, S, Mn, and Zn (Fig. S30), further supporting this source attribution. However, the Mn/Fe ratios observed here (FOS: 0.012; MRS-LCP: 0.006) are lower than those reported by Sylvestre et al. (2017) (0.056). This discrepancy likely reflects differences in particle size fraction (PM_{2.5} in Sylvestre et al., 2017 versus PM₁ in the present study), as well as
500 potential mixing of this factor with other Mn- and Fe-containing sources at MRS-LCP.

Notably, neither railway nor road transport emissions could be attributed to a single PMF factor at MRS-LCP, whereas the St-Charles train station is only approximately 1km (260° direction) from MRS-LCP and the station is located in the city center where massive road traffic occurs (Fig. 1). Nevertheless, the presence of a local contribution (Fig. S15), together with reduced concentrations during weekends (Fig. S17), suggests a partial influence from road transport emissions (Manousakas
505 et al., 2022, 2025) in the Steel Industry factor at MRS-LCP. However, as previously observed at this site (Camman et al., 2024), non-exhaust traffic emissions are only weakly captured in the submicron fraction, since tire and brake wear particles are predominantly associated with particle sizes larger than 1 μm (Bukowiecki et al., 2009; Visser et al., 2015; Pant et al., 2017).

The northwestern and southwestern contributions of the factor at MRS-LCP (Fig. S15), associated with Mistral and sea
510 breezes advection, respectively, suggest a factor primarily related to steel industry emissions originating from the Fos-sur-



Mer industrial area. It was also marked by a sharp increase in diurnal activity between 04:00 and 07:00 UTC, followed by a gradual decline, relative to the onset of sea breeze (Chazeau et al., 2021, Fig. 6). In both cases, oxidation of industrial plumes and secondary sulfate formation from industrial SO₂ emissions can occur (Marris et al., 2012; El Haddad et al., 2013; Chazeau et al., 2021), inducing S factor enrichment and higher average mass contribution of the factor at MRS-LCP (Fig. 3).
515 The additional presence of Pb in the MRS-LCP factor is consistent with previous findings at this site (Camman et al., 2024) and may reflect the inability of PMF to separate Pb-related industrial emissions (4.2.3) from the Steel Industry emissions, due to the spatial proximity of these emission sources.

4.2.5 Zn-Industrial (FOS)

520 A factor composed of Zn > S > K > Fe > Mn > Cu > As, in decreasing order of abundance was identified at FOS (Fig. 4), representing 2.9% of the total elemental PM₁ mass on a yearly average at this site. Airborne Zn has been previously attributed to several sources, including road transport, often associated with Sb (Camman et al., 2024; Manousakas et al., 2025; Charron et al., 2019), industrial processes (Manousakas et al., 2022; Riffault et al., 2015), waste incineration, particularly when associated with Pb and Cl (Moffet et al., 2008; Enestam et al., 2011), and solid fuel combustion (Tissari et al., 2015; Rai et al., 2020). NWR analysis indicated a dominant contribution from the 235°-260° sector (Fig. S16),
525 corresponding to the industrial zone of Fos-sur-Mer, where both a major steel plant and the waste incinerator are located. A minor contribution from the 10°-50° sector suggests influence from land breezes, possibly associated with sea-breeze return flow at night (Drobinski et al., 2007). According to the 2023 French Pollutant Release and Transfer Register (IREP, <https://www.georisques.gouv.fr/donnees/bases-de-donnees/installations-industrielles-rejetant-des-polluants>), the steel plant
530 in Fos-sur-Mer is the largest regional source of Zn emissions. Factor enrichment with Mn further supports its attribution to the steel industry (4.2.4). However, Zn emissions from steelmaking are typically associated with electric arc and basic oxygen furnaces (European Commission, 2008), while the Fos-sur-Mer facility reportedly operates a blast furnace. Furthermore, no correlation was observed between the Zn-Industrial factor and the Steel Industry factor, which may reflect emissions from distinct processes within the same facility. Enrichment in K and S also indicates a potential contribution
535 from waste incineration. Overall, the diverse geographical origins and mixed chemical composition suggest that the Zn-Industrial factor represents a mixing of multiple sources, including steel industry and waste incineration. Despite the clearly distinct sources, PMF was unable to resolve multiple Zn-enriched factors.

4.2.6 Zn-rich (MRS-LCP)

540 A Zn-rich factor, dominated by Zn (53%) with notable contributions from S and K, was identified at MRS-LCP (Fig. 4), accounting on average for 2.5% of the annual PM₁ elemental mass. Its daily cycle (Fig. 6), characterized by morning and evening peaks, is similar to that of Biomass Burning factor (4.2.2) and to road transport rush hours. As discussed in 4.2.5,



various anthropogenic activities can contribute to airborne Zn emissions. However, its northeastern origin under low wind conditions suggests a source advected by nocturnal land-breeze (Chazeau et al., 2021, Fig. S15), ruling out an industrial origin from Fos-sur-Mer (4.2.5). A previous study at MRS-LCP associated a submicron Zn-enriched factor with tire and brake wear, based on the presence of Sb (Cammann et al., 2024). In the present study, Sb was excluded due to a high proportion of measurements BDL (96%). Although Cu can serve as a tracer of non-exhaust traffic emissions (Dubois et al., 2025), the Zn-rich factor shows little enrichment in Cu. This likely reflects the fact that metallic tracers of non-exhaust emissions are predominantly associated with particles larger than 1 μm (Pant et al., 2017). Weak correlations with HOA and BC_{LF} ($R < 0.35$) further exclude road traffic emission as a major contributor (Fig. S24). Instead, the presence of K, similar to the Biomass Burning factor (4.2.2), together with its daily cycle (Fig. 6) and land-breeze transport, point to solid fuel combustion as the dominant source. Nevertheless, its moderate seasonal variability (Fig. S21), its daily cycle (Fig. 6) and substantial contribution to Pb concentrations (34%) can also suggest little influence from waste incineration and non-exhaust traffic emissions.

555

4.2.7 Cl-rich

A Cl-rich factor, composed almost entirely of elemental Cl (FOS: 94%, MRS-LCP: 88%), was identified at both sites and accounted for at least 87% of elemental Cl mass (Fig. 4), and 4.5% and 3.6% of the total elemental mass on a yearly average at FOS and MRS-LCP, respectively. It exhibited a strong seasonal pattern, with low average concentration in summer ($<10 \text{ ng m}^{-3}$ at both sites) and higher average concentration in winter (FOS: 46 ng m^{-3} ; MRS-LCP: 40 ng m^{-3} , Fig. S21). Such seasonality is consistent with previous studies linking fine particulate chloride to combustion-related emissions or secondary formation from gaseous chlorine species (Visser et al., 2015b; Le Breton et al., 2018; Tobler et al., 2020; Rai et al., 2021; Chazeau et al., 2021; Wang et al., 2023; Pawar et al., 2023; Masoud et al., 2023). Primary sources of particulate and gaseous chlorine include biomass burning (e.g. KCl, NH_4Cl), coal combustion, crop residue burning, industrial activities (e.g. Cl-VOCs, steel industry), and sea salt dechlorination (Keene et al., 1999; Wang et al., 2017; Ding et al., 2020; Peng et al., 2021). Chlorine gases may further react with NO_x and N_2O_5 , leading to ClNO_2 formation in particle phase, followed by rapid partitioning into the gas phase (Thornton et al., 2010; Simpson et al., 2015; Le Breton et al., 2018; Ahern et al., 2018). Combustion processes often emit chlorine alongside NO_x , promoting ClNO_2 production. Other reactive intermediates such as Cl_2 and NOCl may also contribute to photochemically active Cl atom formation (Jordan et al., 2015).

The pronounced diurnal variability of the Cl-rich factor, peaking in the early morning and evening, with a sharp increase overnight and minimal activity around midday, indicates rapid ClNO_2 partitioning into the gas phase (Simpson et al., 2015; Faxon et al., 2015; Le Breton et al., 2018; Wang et al., 2022; Wang et al., 2023; Pawar et al., 2023). This daily cycle is also similar to that of the Biomass Burning, BC_{SF} , and chlorinated compounds from the ACSM and AE33 measurements (Fig. 6 & S31). Both seasonal and diurnal behaviours (Fig. 6, S21 & S31) support the attribution of the Cl-rich factor to secondary formation processes from gaseous chlorine species, mainly driven by combustion activities. At FOS, the Cl-rich factor

575



580 correlated with both the Biomass Burning factor ($R^2 = 0.41$, Fig. S32) and Chlorinated Volatile Organic Compounds (Cl-VOCs) associated with industrial activity (1,2-dichloroethyl: $R = 0.57$; tetrachloroethyl: $R = 0.46$, Fig. S26), pointing to a mixed origin. Cl-rich factor originating from various wind directions at both sites (Fig. S15 & S16) further supports a mixed origin of the factor, with a minor northeast contribution suggesting influence from biomass burning transported via nocturnal land breeze. A small contribution from the marine areas may indicate partial influence from sea salt dechlorination, although this was not considered a major source of fine particulate chloride in this study (S6: Sea Salt Dechlorination, Fig. S33-S34).

4.2.8 Br-rich

585 A second halogen-enriched factor was identified at both sites, though with a different composition. The Br-rich factor is primarily composed of S (>57%) and K (>17%), and is highly enriched in Br (88% of Br at both sites) (Fig. 4). It represents 8.3% and 7.4% of the PM_{10} elemental mass on a yearly average at FOS and MRS-LCP, respectively. Its moderate seasonal, diurnal, and weekly variabilities (Fig. 6, S17, S18 & S21), in contrast to the Cl-rich factor (4.2.7), reflects a persistent background contribution, consistent with previous observations at MRS-LCP (Camman et al., 2024). However, similar to the Cl-rich factor, NWR analysis (Fig. S15 & S16) revealed diverse origins for this factor. At both sites, enhanced contributions from marine sectors (south at FOS and southwest at MRS-LCP) suggest a partial influence from marine bromine emissions. In particular, previous work in Fos-sur-Mer area has shown that chlorinated seawater is widely used for industrial cooling and ballast water treatment in cargo vessels, leading to elevated bromoform concentrations at the sea surface in the vicinity of industrial and port activities (from 0.22 to 10.22 $ng\ m^{-3}$; Quivet et al., 2022). A similar practice in passenger vessels may occur at Marseille harbour. Reactive bromine species can then undergo atmospheric reactions to form particulate brominated compounds (Kothai et al., 2011; Simpson et al., 2015). At FOS, the southwestern origin also corresponds to the port-industrial area hosting a coal-powered blast furnace, suggesting a potential contribution from particulate Br formed via reactive bromine gases emitted during coal combustion (Lee et al., 2018; Rai et al., 2021; Peng et al., 2021).

590 At MRS-LCP, the Br-rich factor showed a major contribution from the southeast sector (105° - 135°) under elevated wind speeds, corresponding to two synoptic regimes: Sirocco (removed from the dataset, 3.1, Fig. S5) and the “Marine” wind, typically observed during fall and spring (Chazeau et al., 2021). Although observed only occasionally, the “Marine” wind travelled extensively over the Mediterranean Sea, potentially contributing to the sulfur and bromine enrichment of this factor. Another potential contributor is a chemical facility located approximately 10 km east of MRS-LCP, along the 105° sector (Fig. 1), which has reported bromine use and past incidents involving gaseous bromine leaks (bouches-du-rhône.data.gouv.fr, 2013; <https://www.georisques.gouv.fr>). Finally, minor contributions from the northeast sector (5° - 90°) suggest aerosol nocturnal transport with sea-breeze return flow, similar to the Zn-rich and the Cl-rich factors (4.2.6 and 4.2.7) (Drobinski et al., 2007), further supporting the secondary origin of this factor.



4.2.9 S-rich

The S-rich factor is by far the most abundant (Fig. 3), contributing to more than 50% of the total measured elemental mass on a yearly average for both sites. It is mainly composed with S (95%), elevated Se traces (approximately 35% of Se) at both sites, and accounts for 73% and 79% of elemental S mass at FOS and MRS-LCP, respectively (Fig. 4). The S-rich aerosols are typically attributed to oxidation of SO₂ to sulfate (SO₄²⁻) or to direct sulfate emission (Visser et al., 2015b; Rai et al., 2020a, 2020b; Rai et al., 2021; Manousakas et al., 2022, 2025). S-enriched factors are often associated with Se (Weber et al., 2019), as both elements share major anthropogenic sources, such as metals production, coal, fuel, and biomass combustion, as well as natural sources such as sea salt and volcanic activity (Eldred, 1997; Kuittinen et al., 2024; Su et al., 2025). Both elements are primarily emitted into gas phase then converted to particulate forms at different rates, leading to decreasing Se/S ratios with aerosol ageing (Zhuang et al., 1999; Wen & Carignan, 2007; Liu et al., 2021). In this study, Se/S ratios were 1.9×10^{-4} at FOS and 1.2×10^{-4} at MRS-LCP, within the lower range of previously reported values (1.7×10^{-4} in PM_{2.5}, Kumar et al., 2025; 3.2×10^{-4} in PM₁₀, Rai et al., 2020b). In the area, the only identified coal combustion source is the blast furnace of the steel industry in Fos-sur-Mer, but those ratios suggest limited influence from coal combustion emissions.

NWR analysis points to a dominant contribution from the sea at both sites (Fig. S15 & S16), consistent with particulate S emissions from shipping and sea water, or secondary formation in the port-areas of the Marseille-Fos basin. Previous work at MRS-LCP reported elevated sulfate levels from major shipping routes, highlighting the continued importance of shipping emissions in sulfate production (Chazeau et al., 2021), even after SO₂ reductions (4.2.1).

Assuming all S is in the form of SO₄²⁻, reconstructed sulfate from elemental S (Xact) strongly correlates with non-refractory SO₄²⁻ from ToF-ACSM (R² = 0.91, slope = 0.99; Fig. S35). This confirms that sulfates are the dominant particulate form of sulfur measured by the Xact, in line with findings across Europe (Furger et al., 2017: R² = 0.85, slope = 1.32, Xact in PM₁₀ and ACSM in PM₁; Tremper et al., 2018: R² = 0.93, slope = 1.41, Xact in PM_{2.5} and ACSM in PM₁). The larger slopes observed in previous studies likely reflect differences in particle size fractions sampled by the Xact and ACSM instruments, while operating both instruments in PM₁ led to reduced size-related biases in this study. Time series at both sites and ToF-ACSM SO₄²⁻ at MRS-LCP indicate an optimal sulfate production period from January to mid-October, followed by a sharp decline, likely linked to a sudden meteorological shift after a Sirocco event in mid-October (Fig. S36). Seasonal and diurnal patterns (enhanced activity between 10:00-15:00 UTC, coinciding with peak solar radiation; Fig. 6 & S36) confirm that this factor is strongly driven by secondary sulfate formation under high photochemical activity and stagnant conditions (El Haddad et al., 2013; Salameh et al., 2015; Chazeau et al., 2021).

4.2.10 Dust

The Dust factor is primarily composed of Ca (>50%), with significant contributions from Ti at both sites (FOS: 51%, MRS-LCP: 35%), alongside contributions of S, Fe, and K (Fig. 4). Although crustal material is generally associated with coarse



640 particles (Pey et al., 2013), mechanical processes such as sandblasting may also explain its presence in the PM₁ fraction (Gomes et al., 1990). However, this factor contributed only modestly to PM₁ elemental aerosol mass (<5%) at both sites (Fig. 3).

Dust can refer to various sources, including: a) Short-range resuspension dust, linked to road dust or construction activities (Belis et al., 2011; Dall'Osto et al., 2013; Visser et al., 2015b; Manousakas et al., 2022), b) Medium-range transported dust
645 such as industrial dust (Riffault et al., 2015, Almeida et al., 2020) or construction dust, and c) Long-range transport of crustal material with strong wind regimes like the Mistral or Sirocco (Flaounas et al., 2009). NWR analyses at both sites point to a dominant contribution from crustal material transported during Mistral episodes (275°-360° sector, Fig. S15 & S16). However, the observed diurnal and weekly patterns display daytime peaks predominantly on weekdays, consistent with local resuspension processes driven by road traffic (Fig. 6, S17 & S18). These cycles are also similar to those of the Steel Industry
650 factor at both sites (4.2.4), suggesting possible partial mixing between the two sources. This is also supported by the partial 235°-260° sector origin of the factor at FOS, and by the reported elevated Ca concentrations downwind of the blast furnace unit at the Fos-sur-Mer steel industry facility (Sylvestre et al., 2017, Fig. S16 & S30). This is consistent with previous findings indicating a mixture of dust and steel industry emissions, obtained with source apportionment approach (Taiwo et al., 2014b).

655 **5 Conclusion**

This year-long source apportionment study at two sites provides a comprehensive picture of submicron elemental aerosols across the Marseille-Fos basin using high-resolution Xact PM₁ measurements combined with a dynamic rolling PMF approach. The sites, MRS-LCP (urban background) and FOS (industrial), are located on opposite sides of the basin, and are influenced by complex regional meteorological conditions that facilitate inter-site aerosol transport. A novel dynamic source
660 apportionment approach was applied using a 21-day rolling window PMF via the SoFi Pro toolkit. This dynamic framework allowed a more realistic representation of changing emission patterns compared with a static PMF and atmospheric processes in a complex coastal-industrial environment characterized by frequent wind shifts and inter-site air mass exchanges.

The analysis resolved nine PMF factors at FOS and eight at MRS-LCP, with seven factors common to both sites. Among these seven factors, three were attributed to secondary aerosol formation: S-rich factor (FOS: 52%, MRS-LCP: 60.3%), Cl-rich (FOS: 4.5%, MRS-LCP: 3.6%), and Br-rich (FOS: 8.3%, MRS-LCP: 7.4%). Biomass burning was the second-largest
665 contributor at both sites (FOS: 14%, MRS-LCP: 12.5%). As expected given the intense harbour activity in the region, a shipping factor was identified (FOS: 6.7%, MRS-LCP: 3.3%), with episodic peaks exceeding 400 ng m⁻³ that can last 1-3 hours. A dust-related factor, linked to both long-range transport and local resuspension, was also observed at both sites (FOS: 4.3%, MRS-LCP: 3.5%). A non-ascribed Zn-rich factor was retrieved exclusively at MRS-LCP (2.5%), while two
670 additional industrial factors were resolved only at FOS: a Pb-Industrial factor (2.7%) and a Zn-Industrial factor (2.9%), associated with waste incineration and steel production. A Steel Industry factor was also identified at MRS-LCP (6.9%),



though with differences in composition. These differences suggest both mixing of industrial emissions and the formation of secondary aerosols during plume transport from FOS to MRS-LCP. These results clearly demonstrate that emissions from the Fos-sur-Mer industrial area influence air quality throughout the basin, transported under alternating Mistral and sea-land
675 breeze regimes.

Ten distinct elemental sources were characterized in the MRS-FOS basin, five of which (Shipping, Biomass Burning, Pb-Industrial, Zn-Industrial, and Steel Industry) stem directly from primary anthropogenic emissions. The predominance of human-related sources underscores the strong industrial and maritime imprint on the region's atmospheric composition. This issue is further amplified by the basin's topography and population density, which enhance population exposure to a
680 complex mixture of potentially harmful airborne elements. Considering recent epidemiological findings linking residence near the Berre industrial zone with increased chronic disease prevalence, including cancer and diabetes (Jeanjean et al., 2022), the present results call for closer integration between atmospheric chemistry and health research. Future studies should focus on the toxic potential of these resolved submicron sources to better quantify their public health implications in industrialized coastal regions.

685 **Financial support**

This study received funding from the French Agence Nationale de la Recherche (ANR) programme under grant agreement no. ANR-21-CE22-0015 (SHIPAIR). This study was also supported by AtmoSud for funding analytical instruments.

Data availability

All the Rolling PMF Xact results from this work can be accessed through Zenodo:
690 https://zenodo.org/records/18374331?preview=1&token=eyJhbGciOiJIUzUxMiIsImhhdCI6MTc2OTQyMjU3NywiZXhwIjo4Nzk4Njc1MTk5fQ.eyJpZCI6IjMjA5Y2EyLWl4MTgtNGY5OS05OGE1LTZmODEzZmZlMjU4OSIsImRhdGEiOiOnt9LCJyYW5kb20iOiI4ZDZjNzdiM2IxYzQ1NTNjY2VIOWY2NTc1Y2F1OWFkMiJ9.NS24rtFIWO69UgWBLj1GMT8ZlPx1z7_zgOkPO8qTs6auczRuKN8xJ5_avWt48Sx5bbPZIED3S2faC0cuIvcRCA (preview link).

Code availability

The PD-SID and CD code used in this work can be accessed through Zenodo:
695 https://zenodo.org/records/18374331?preview=1&token=eyJhbGciOiJIUzUxMiIsImhhdCI6MTc2OTQzNDkyMSwiZXhwIjo4Nzk4Njc1MTk5fQ.eyJpZCI6IjdlN2ZlMzllLWY5NWUtNGU4NS04YTUyLWl4MTc2OTQzNDkyMSwiImRhdGEiOiOnt9LCJyYW5kb20iOiI0ZDdjZWQ1MGVhYzA4NDkyYTM1YWJiY2VkNTliMDY2ZiJ9.Z_BiknPu-cS7-HVb6kMgWxmKRh4QYrjsRvbS4k8bw20gs1P28oPc5dzMm1ufNhsF4sHN3J_e9cWYqpBR6LcjqVQ (preview link).



700 **Author contributions**

MB, BC, NM, JLJ, GU, and BDA conceived the study. AD, GG, and RB provided technical assistance during the experiments. AP provided the Xact instrument used for measurements at the FOS site. RB supported the deployment of the Xact instrument at the FOS measurement site. AD contributed to the Xact data analysis. BC conducted the ToF-ACSM data analysis. MB conducted the Xact data analysis and wrote the paper, with contributions from all of the co-authors.

705 **Competing interests**

The contact author has declared that none of the authors has any competing interests.

Acknowledgements

The authors would like to thank AtmoSud technical team and Brice Temime-Roussel for instrument maintenance and calibration at the FOS and MRS-LCP stations. Mathilde Brezins also would like to thank Anna Tobler and Francesco Canonaco for their regular support and assistance with SoFi toolkit debugging. Mathilde Brezins acknowledges the use of the ChatGPT AI tool for Python script correction and for proofreading and grammar improvement during the manuscript preparation. All outputs were reviewed and edited by Mathilde Brezins, who takes full responsibility for the final content. All of the final wording reflects Mathilde Brezins's own edits and judgement.

References

- 715 Ahern, A. T., Goldberger, L., Jahl, L., Thornton, J., and Sullivan, R. C.: Production of N_2O_5 and ClNO_2 through Nocturnal Processing of Biomass-Burning Aerosol, *Environ. Sci. Technol.*, 52, 550–559, <https://doi.org/10.1021/acs.est.7b04386>, 2018.
- Alastuey, A., Querol, X., Aas, W., Lucarelli, F., Pérez, N., Moreno, T., Cavalli, F., Areskou, H., Balan, V., Catrambone, M., Ceburnis, D., Cerro, J. C., Conil, S., Gevorgyan, L., Hueglin, C., Imre, K., Jaffrezo, J.-L., Leeson, S. R., Mihalopoulos, N., Mitisinkova, M., O'Dowd, C. D., Pey, J., Putaud, J.-P., Riffault, V., Ripoll, A., Sciare, J., Sellegri, K., Spindler, G., and Yttri, K. E.: Geochemistry of PM_{10} over Europe during the EMEP intensive measurement periods in summer 2012 and winter 2013, *Atmos. Chem. Phys.*, 16, 6107–6129, <https://doi.org/10.5194/acp-16-6107-2016>, 2016.
- Almeida, S. M., Lage, J., Fernández, B., Garcia, S., Reis, M. A., and Chaves, P. C.: Chemical characterization of atmospheric particles and source apportionment in the vicinity of a steelmaking industry, *Science of The Total Environment*, 725 521–522, 411–420, <https://doi.org/10.1016/j.scitotenv.2015.03.112>, 2015.



- Almeida, S. M., Manousakas, M., Diapouli, E., Kertesz, Z., Samek, L., Hristova, E., Šega, K., Alvarez, R. P., Belis, C. A., and Eleftheriadis, K.: Ambient particulate matter source apportionment using receptor modelling in European and Central Asia urban areas, *Environmental Pollution*, 266, 115199, <https://doi.org/10.1016/j.envpol.2020.115199>, 2020.
- 730 Belis, C. A., Cancelinha, J., Duane, M., Forcina, V., Pedroni, V., Passarella, R., Tanet, G., Douglas, K., Piazzalunga, A., Bolzacchini, E., Sangiorgi, G., Perrone, M.-G., Ferrero, L., Fermo, P., and Larsen, B. R.: Sources for PM air pollution in the Po Plain, Italy: I. Critical comparison of methods for estimating biomass burning contributions to benzo(a)pyrene, *Atmospheric Environment*, 45, 7266–7275, <https://doi.org/10.1016/j.atmosenv.2011.08.061>, 2011.
- 735 Belis, C. A., Pernigotti, D., Karagulian, F., Pirovano, G., Larsen, B. R., Gerboles, M., and Hopke, P. K.: A new methodology to assess the performance and uncertainty of source apportionment models in intercomparison exercises, *Atmospheric Environment*, 119, 35–44, <https://doi.org/10.1016/j.atmosenv.2015.08.002>, 2015.
- Borlaza, L. J. S., Weber, S., Uzu, G., Jacob, V., Cañete, T., Micallef, S., Trébuchon, C., Slama, R., Favez, O., and Jaffrezo, J.-L.: Disparities in particulate matter (PM₁₀) origins and oxidative potential at a city scale (Grenoble, France) – Part 1: Source apportionment at three neighbouring sites, *Atmos. Chem. Phys.*, 21, 5415–5437, <https://doi.org/10.5194/acp-21-5415-2021>, 2021.
- 740 Bougiatioti, A., Stavroulas, I., Kostenidou, E., Zarnpas, P., Theodosi, C., Kouvarakis, G., Canonaco, F., Prévôt, A. S. H., Nenes, A., Pandis, S. N., and Mihalopoulos, N.: Processing of biomass-burning aerosol in the eastern Mediterranean during summertime, *Atmos. Chem. Phys.*, 14, 4793–4807, <https://doi.org/10.5194/acp-14-4793-2014>, 2014.
- Bourtsoukidis, E., Pozzer, A., Williams, J., Makowski, D., Peñuelas, J., Matthaios, V. N., Lazoglou, G., Yañez-Serrano, A. M., Lelieveld, J., Ciais, P., Vrekoussis, M., Daskalakis, N., and Sciare, J.: High temperature sensitivity of monoterpene emissions from global vegetation, *Commun Earth Environ*, 5, 23, <https://doi.org/10.1038/s43247-023-01175-9>, 2024.
- 745 Bozzetti, C., El Haddad, I., Salameh, D., Daellenbach, K. R., Fermo, P., Gonzalez, R., Minguillón, M. C., Iinuma, Y., Poulain, L., Elser, M., Müller, E., Slowik, J. G., Jaffrezo, J.-L., Baltensperger, U., Marchand, N., and Prévôt, A. S. H.: Organic aerosol source apportionment by offline-AMS over a full year in Marseille, *Atmos. Chem. Phys.*, 17, 8247–8268, <https://doi.org/10.5194/acp-17-8247-2017>, 2017.
- 750 Bukowiecki, N., Lienemann, P., Hill, M., Furger, M., Richard, A., Amato, F., Prévôt, A. S. H., Baltensperger, U., Buchmann, B., and Gehrig, R.: PM₁₀ emission factors for non-exhaust particles generated by road traffic in an urban street canyon and along a freeway in Switzerland, *Atmospheric Environment*, 44, 2330–2340, <https://doi.org/10.1016/j.atmosenv.2010.03.039>, 2010.
- 755 Cadeo, L., Biffi, B., Chazeau, B., Colombi, C., Cosenza, R., Cuccia, E., Manousakas, M.-I., Daellenbach, K. R., Prévôt, A. S. H., and Vecchi, R.: Intercomparison of online and offline XRF spectrometers for determining the PM₁₀ elemental composition of ambient aerosol, <https://doi.org/10.5194/egusphere-2025-110>, 11 March 2025.
- Camman, J., Chazeau, B., Marchand, N., Durand, A., Gille, G., Lanzi, L., Jaffrezo, J.-L., Wortham, H., and Uzu, G.: Oxidative potential apportionment of atmospheric PM₁₀: A new approach combining high-sensitive online analysers for



- chemical composition and offline OP measurement technique, *Aerosols/Atmospheric Modelling and Data Analysis/Troposphere/Chemistry (chemical composition and reactions)*, <https://doi.org/10.5194/egusphere-2023-1441>, 2024.
- 760 Canonaco, F., Crippa, M., Slowik, J. G., Baltensperger, U., and Prévôt, A. S. H.: SoFi, an IGOR-based interface for the efficient use of the generalized multilinear engine (ME-2) for the source apportionment: ME-2 application to aerosol mass spectrometer data, *Atmos. Meas. Tech.*, 6, 3649–3661, <https://doi.org/10.5194/amt-6-3649-2013>, 2013.
- 765 Canonaco, F., Tobler, A., Chen, G., Sosedova, Y., Slowik, J. G., Bozzetti, C., Daellenbach, K. R., El Haddad, I., Crippa, M., Huang, R.-J., Furger, M., Baltensperger, U., and Prévôt, A. S. H.: A new method for long-term source apportionment with time-dependent factor profiles and uncertainty assessment using SoFi Pro: application to 1 year of organic aerosol data, *Atmos. Meas. Tech.*, 14, 923–943, <https://doi.org/10.5194/amt-14-923-2021>, 2021.
- 770 Charron, A., Polo-Rehn, L., Besombes, J.-L., Golly, B., Buisson, C., Chanut, H., Marchand, N., Guillaud, G., and Jaffrezo, J.-L.: Identification and quantification of particulate tracers of exhaust and non-exhaust vehicle emissions, *Atmos. Chem. Phys.*, 19, 5187–5207, <https://doi.org/10.5194/acp-19-5187-2019>, 2019.
- Chazeau, B., Temime-Roussel, B., Gille, G., Mesbah, B., D’Anna, B., Wortham, H., and Marchand, N.: Measurement report: Fourteen months of real-time characterisation of the submicronic aerosol and its atmospheric dynamics at the Marseille–Longchamp supersite, *Atmos. Chem. Phys.*, 21, 7293–7319, <https://doi.org/10.5194/acp-21-7293-2021>, 2021.
- 775 Chazeau, B., El Haddad, I., Canonaco, F., Temime-Roussel, B., D’Anna, B., Gille, G., Mesbah, B., Prévôt, A. S. H., Wortham, H., and Marchand, N.: Organic aerosol source apportionment by using rolling positive matrix factorization: Application to a Mediterranean coastal city, *Atmospheric Environment: X*, 14, 100176, <https://doi.org/10.1016/j.aeaoa.2022.100176>, 2022.
- Chebaicheb, H., F. De Brito, J., Chen, G., Tison, E., Marchand, C., Prévôt, A. S. H., Favez, O., and Riffault, V.: Investigation of four-year chemical composition and organic aerosol sources of submicron particles at the ATOLL site in northern France, *Environmental Pollution*, 330, 121805, <https://doi.org/10.1016/j.envpol.2023.121805>, 2023.
- 780 Chen, G., Sosedova, Y., Canonaco, F., Fröhlich, R., Tobler, A., Vlachou, A., Daellenbach, K. R., Bozzetti, C., Hueglin, C., Graf, P., Baltensperger, U., Slowik, J. G., El Haddad, I., and Prévôt, A. S. H.: Time-dependent source apportionment of submicron organic aerosol for a rural site in an alpine valley using a rolling positive matrix factorisation (PMF) window, *Atmos. Chem. Phys.*, 21, 15081–15101, <https://doi.org/10.5194/acp-21-15081-2021>, 2021.
- 785 Chen, G., Canonaco, F., Tobler, A., Aas, W., Alastuey, A., Allan, J., Atabakhsh, S., Aurela, M., Baltensperger, U., Bougiatioti, A., De Brito, J. F., Ceburnis, D., Chazeau, B., Chebaicheb, H., Daellenbach, K. R., Ehn, M., El Haddad, I., Eleftheriadis, K., Favez, O., Flentje, H., Font, A., Fossom, K., Freney, E., Gini, M., Green, D. C., Heikkinen, L., Herrmann, H., Kalogridis, A.-C., Keernik, H., Lhotka, R., Lin, C., Lunder, C., Maasikmets, M., Manousakas, M. I., Marchand, N., Marin, C., Marmureanu, L., Mihalopoulos, N., Močnik, G., Nęcki, J., O’Dowd, C., Ovadnevaite, J., Peter, T., Petit, J.-E.,
- 790 Pikridas, M., Matthew Platt, S., Pokorná, P., Poulain, L., Priestman, M., Riffault, V., Rinaldi, M., Róžański, K., Schwarz, J., Sciare, J., Simon, L., Skiba, A., Slowik, J. G., Sosedova, Y., Stavroulas, I., Styszko, K., Teinmaa, E., Timonen, H., Tremper, A., Vasilescu, J., Via, M., Vodička, P., Wiedensohler, A., Zografou, O., Cruz Minguillón, M., and Prévôt, A. S. H.:



- European aerosol phenomenology – 8: Harmonised source apportionment of organic aerosol using 22 Year-long ACSM/AMS datasets, *Environment International*, 166, 107325, <https://doi.org/10.1016/j.envint.2022.107325>, 2022a.
- 795 Chen, G., Canonaco, F., Slowik, J. G., Daellenbach, K. R., Tobler, A., Petit, J.-E., Favez, O., Stavroulas, I., Mihalopoulos, N., Gerasopoulos, E., El Haddad, I., Baltensperger, U., and Prévôt, A. S. H.: Real-Time Source Apportionment of Organic Aerosols in Three European Cities, *Environ. Sci. Technol.*, 56, 15290–15297, <https://doi.org/10.1021/acs.est.2c02509>, 2022b.
- Chevet, E., Boiron, O., and Anselmet, F.: Modeling of air pollution due to marine traffic in Marseille, *Atmospheric Environment*, 329, 120542, <https://doi.org/10.1016/j.atmosenv.2024.120542>, 2024.
- 800 Clements, N., Eav, J., Xie, M., Hannigan, M. P., Miller, S. L., Navidi, W., Peel, J. L., Schauer, J. J., Shafer, M. M., and Milford, J. B.: Concentrations and source insights for trace elements in fine and coarse particulate matter, *Atmospheric Environment*, 89, 373–381, <https://doi.org/10.1016/j.atmosenv.2014.01.011>, 2014.
- Dall’Osto, M., Querol, X., Amato, F., Karanasiou, A., Lucarelli, F., Nava, S., Calzolari, G., and Chiari, M.: Hourly elemental concentrations in PM_{2.5} aerosols sampled simultaneously at urban background and road site during SAPUSS – diurnal variations and PMF receptor modelling, *Atmos. Chem. Phys.*, 13, 4375–4392, <https://doi.org/10.5194/acp-13-4375-2013>, 2013.
- 805 Dockery DW, Pope CA 3rd, Xu X, Spengler JD, Ware JH, Fay ME, Ferris BG Jr, Speizer FE. An association between air pollution and mortality in six U.S. cities. *N Engl J Med.* 1993 Dec 9;329(24):1753-9. doi: 10.1056/NEJM199312093292401. PMID: 8179653.
- 810 Ding, X., Li, Q., Wu, D., Huo, Y., Liang, Y., Wang, H., Zhang, J., Wang, S., Wang, T., Ye, X., and Chen, J.: Gaseous and Particulate Chlorine Emissions From Typical Iron and Steel Industry in China, *JGR Atmospheres*, 125, e2020JD032729, <https://doi.org/10.1029/2020JD032729>, 2020.
- Drinovec, L., Močnik, G., Zotter, P., Prévôt, A. S. H., Ruckstuhl, C., Coz, E., Rupakheti, M., Sciare, J., Müller, T., Wiedensohler, A., and Hansen, A. D. A.: The “dual-spot” Aethalometer: an improved measurement of aerosol black carbon with real-time loading compensation, *Atmos. Meas. Tech.*, 8, 1965–1979, <https://doi.org/10.5194/amt-8-1965-2015>, 2015.
- 815 Drobinski, P., Saïd, F., Ancellet, G., Arteta, J., Augustin, P., Bastin, S., Brut, A., Caccia, J. L., Campistron, B., Cautenet, S., Colette, A., Coll, I., Corsmeier, U., Cros, B., Dabas, A., Delbarre, H., Dufour, A., Durand, P., Guénard, V., Hasel, M., Kalthoff, N., Kottmeier, C., Lasry, F., Lemonsu, A., Lohou, F., Masson, V., Menut, L., Moppert, C., Peuch, V. H., Puygrenier, V., Reitebuch, O., and Vautard, R.: Regional transport and dilution during high-pollution episodes in southern France: Summary of findings from the Field Experiment to Constraint Models of Atmospheric Pollution and Emissions Transport (ESCOMPTE), *J. Geophys. Res.*, 112, 2006JD007494, <https://doi.org/10.1029/2006JD007494>, 2007.
- 820 Dubois, N., Foret, G., Siour, G., Uzu, G., Couvidat, F., Vida, M., André, J.-M., Moukhtar, S., Sirina-Leboine, N., Aujay-Plouzeau, R., Alleman, L., Conil, S., Pallares, C., Salque-Moreton, G., Stratigou, E., Alastuey, A., Querol, X., Ito, A.,



- Jaffrezo, J.-L., Favez, O., and Beekmann, M.: Construction of copper, iron and manganese anthropogenic emission inventories for Europe, *Atmospheric Environment*, 363, 121582, <https://doi.org/10.1016/j.atmosenv.2025.121582>, 2025.
- Dufresne, M., Salameh, T., Leonardis, T., Gille, G., Armengaud, A., and Sauvage, S.: Volatile organic compound sources and impacts in an urban Mediterranean area (Marseille, France), *Atmos. Chem. Phys.*, 25, 5977–5999, 830 <https://doi.org/10.5194/acp-25-5977-2025>, 2025.
- Efron, B. “Bootstrap Methods: Another Look at the Jackknife.” *The Annals of Statistics*, vol. 7, no. 1, pp. 1–26. JSTOR, <http://www.jstor.org/stable/2958830>, 1979.
- El Haddad, I., Marchand, N., Temime-Roussel, B., Wortham, H., Piot, C., Besombes, J.-L., Baduel, C., Voisin, D., Armengaud, A., and Jaffrezo, J.-L.: Insights into the secondary fraction of the organic aerosol in a Mediterranean urban area: 835 Marseille, *Atmos. Chem. Phys.*, 11, 2059–2079, <https://doi.org/10.5194/acp-11-2059-2011>, 2011.
- El Haddad, I., D’Anna, B., Temime-Roussel, B., Nicolas, M., Boreave, A., Favez, O., Voisin, D., Sciare, J., George, C., Jaffrezo, J.-L., Wortham, H., and Marchand, N.: Towards a better understanding of the origins, chemical composition and aging of oxygenated organic aerosols: case study of a Mediterranean industrialized environment, Marseille, *Atmos. Chem. Phys.*, 13, 7875–7894, <https://doi.org/10.5194/acp-13-7875-2013>, 2013.
- 840 Eldred, R. A.: Comparison of Selenium and Sulfur at Remote Sites, *Journal of the Air & Waste Management Association*, 47, 204–211, <https://doi.org/10.1080/10473289.1997.10464423>, 1997.
- Enestam, S., Boman, C., Niemi, J., Boström, D., Backman, R., Mäkelä, K., and Hupa, M.: Occurrence of Zinc and Lead in Aerosols and Deposits in the Fluidized-Bed Combustion of Recovered Waste Wood. Part 1: Samples from Boilers, *Energy Fuels*, 25, 1396–1404, <https://doi.org/10.1021/ef101478n>, 2011.
- 845 European Commission. Joint Research Centre. Institute for Environment and Sustainability: The Krakow receptor modelling inter-comparison exercise, Publications Office, LU, 2008.
- Faxon, C., Bean, J., and Ruiz, L.: Inland Concentrations of Cl₂ and ClNO₂ in Southeast Texas Suggest Chlorine Chemistry Significantly Contributes to Atmospheric Reactivity, *Atmosphere*, 6, 1487–1506, <https://doi.org/10.3390/atmos6101487>, 2015.
- 850 Flaounas, E., Coll, I., Armengaud, A., and Schmechtig, C.: The representation of dust transport and missing urban sources as major issues for the simulation of PM episodes in a Mediterranean area, *Atmos. Chem. Phys.*, 2009.
- Formenti, P., Nava, S., Prati, P., Chevaillier, S., Klaver, A., Lafon, S., Mazzei, F., Calzolari, G., and Chiari, M.: Self-attenuation artifacts and correction factors of light element measurements by X-ray analysis: Implication for mineral dust composition studies, *J. Geophys. Res.*, 115, 2009JD012701, <https://doi.org/10.1029/2009JD012701>, 2010.
- 855 Fossum, K. N., Lin, C., O’Sullivan, N., Lei, L., Hellebust, S., Ceburnis, D., Afzal, A., Tremper, A., Green, D., Jain, S., Byčenkienė, S., O’Dowd, C., Wenger, J., and Ovadnevaite, J.: Two distinct ship emission profiles for organic-sulfate source apportionment of PM in sulfur emission control areas, *Atmos. Chem. Phys.*, 24, 10815–10831, <https://doi.org/10.5194/acp-24-10815-2024>, 2024.



- Fröhlich, R., Cubison, M. J., Slowik, J. G., Bukowiecki, N., Prévôt, A. S. H., Baltensperger, U., Schneider, J., Kimmel, J. R.,
860 Gonin, M., Rohner, U., Worsnop, D. R., and Jayne, J. T.: The ToF-ACSM: a portable aerosol chemical speciation monitor
with TOFMS detection, *Atmos. Meas. Tech.*, 6, 3225–3241, <https://doi.org/10.5194/amt-6-3225-2013>, 2013.
- Fuller, R., Landrigan, P. J., Balakrishnan, K., Bathan, G., Bose-O'Reilly, S., Brauer, M., Caravanos, J., Chiles, T., Cohen,
A., Corra, L., Cropper, M., Ferraro, G., Hanna, J., Hanrahan, D., Hu, H., Hunter, D., Janata, G., Kupka, R., Lanphear, B.,
Lichtveld, M., Martin, K., Mustapha, A., Sanchez-Triana, E., Sandilya, K., Schaeffli, L., Shaw, J., Seddon, J., Suk, W.,
865 Téllez-Rojo, M. M., and Yan, C.: Pollution and health: a progress update, *The Lancet Planetary Health*, 6, e535–e547,
[https://doi.org/10.1016/S2542-5196\(22\)00090-0](https://doi.org/10.1016/S2542-5196(22)00090-0), 2022.
- Furger, M., Minguillón, M. C., Yadav, V., Slowik, J. G., Hüglin, C., Fröhlich, R., Petterson, K., Baltensperger, U., and
Prévôt, A. S. H.: Elemental composition of ambient aerosols measured with high temporal resolution using an online XRF
spectrometer, *Atmos. Meas. Tech.*, 10, 2061–2076, <https://doi.org/10.5194/amt-10-2061-2017>, 2017.
- 870 Gomes, L., Bergametti, G., Coudé-Gaussen, G., and Rognon, P.: Submicron desert dusts: A sandblasting process, *J.*
Geophys. Res., 95, 13927–13935, <https://doi.org/10.1029/JD095iD09p13927>, 1990.
- Gomez, J., Allen, R. J., Turnock, S. T., Horowitz, L. W., Tsigaridis, K., Bauer, S. E., Olivie, D., Thomson, E. S., and
Ginoux, P.: The projected future degradation in air quality is caused by more abundant natural aerosols in a warmer world,
Commun Earth Environ, 4, 22, <https://doi.org/10.1038/s43247-023-00688-7>, 2023.
- 875 Heikkinen, L., Äijälä, M., Daellenbach, K. R., Chen, G., Garmash, O., Aliaga, D., Graeffe, F., Rätty, M., Luoma, K., Aalto,
P., Kulmala, M., Petäjä, T., Worsnop, D., and Ehn, M.: Eight years of sub-micrometre organic aerosol composition data
from the boreal forest characterized using a machine-learning approach, *Atmos. Chem. Phys.*, 21, 10081–10109,
<https://doi.org/10.5194/acp-21-10081-2021>, 2021.
- Janhall, S., Andreae, M. O., and Poschl, U.: Biomass burning aerosol emissions from vegetation fires: particle number and
880 mass emission factors and size distributions, *Atmos. Chem. Phys.*, 2010.
- Jeanjean, M., Dron, J., Allen, B. L., Gramaglia, C., Austruy, A., Lees, J., Ferrier, Y., Periot, M., Dotson, M. P., Chamaret, P.,
and Cohen, A. K.: Participatory environmental health research: A tool to explore the socio-exposome in a major european
industrial zone, *Environmental Research*, 218, 114865, <https://doi.org/10.1016/j.envres.2022.114865>, 2023.
- Jézéquel, A., Faranda, D., Drobinski, P., and Lionello, P.: Extreme Event Attribution in the Mediterranean, *Intl Journal of*
885 *Climatology*, e8799, <https://doi.org/10.1002/joc.8799>, 2025.
- Jonsson, Å. M., Westerlund, J., and Hallquist, M.: Size-resolved particle emission factors for individual ships: PARTICLE
EFs FROM INDIVIDUAL SHIPS, *Geophys. Res. Lett.*, 38, n/a-n/a, <https://doi.org/10.1029/2011GL047672>, 2011.
- Jordan, C. E., Pszenny, A. A. P., Keene, W. C., Cooper, O. R., Deegan, B., Maben, J., Routhier, M., Sander, R., and Young,
890 A. H.: Origins of aerosol chlorine during winter over north central Colorado, USA, *JGR Atmospheres*, 120, 678–694,
<https://doi.org/10.1002/2014JD022294>, 2015.



- Keene, William. C., Khalil, M. A. K., Erickson, David. J., McCulloch, A., Graedel, T. E., Lobert, J. M., Aucott, M. L., Gong, S. L., Harper, D. B., Kleiman, G., Midgley, P., Moore, R. M., Seuzaret, C., Sturges, W. T., Benkovitz, C. M., Koropalov, V., Barrie, L. A., and Li, Y. F.: Composite global emissions of reactive chlorine from anthropogenic and natural sources: Reactive Chlorine Emissions Inventory, *J. Geophys. Res.*, 104, 8429–8440, <https://doi.org/10.1029/1998JD100084>, 1999.
- Kfoury, A., Ledoux, F., Roche, C., Delmaire, G., Roussel, G., and Courcot, D.: PM_{2.5} source apportionment in a French urban coastal site under steelworks emission influences using constrained non-negative matrix factorization receptor model, *Journal of Environmental Sciences*, 40, 114–128, <https://doi.org/10.1016/j.jes.2015.10.025>, 2016.
- Kothai, P., Saradhi, I. V., Pandit, G. G., Markwitz, A., and Puranik, V. D.: Chemical Characterization and Source Identification of Particulate Matter at an Urban Site of Navi Mumbai, India, *Aerosol Air Qual. Res.*, 11, 560–569, <https://doi.org/10.4209/aaqr.2011.02.0017>, 2011.
- Kreyling, W. G., Semmler-Behnke, M., and Möller, W.: Ultrafine Particle–Lung Interactions: Does Size Matter?, *Journal of Aerosol Medicine*, 19, 74–83, <https://doi.org/10.1089/jam.2006.19.74>, 2006.
- Kuittinen, N., Timonen, H., Karjalainen, P., Murtonen, T., Vesala, H., Bloss, M., Honkanen, M., Lehtoranta, K., Aakko-Saksa, P., and Rönkkö, T.: In-depth characterization of exhaust particles performed on-board a modern cruise ship applying a scrubber, *Science of The Total Environment*, 946, 174052, <https://doi.org/10.1016/j.scitotenv.2024.174052>, 2024.
- Kumar, S., Aggarwal, S. G., Gupta, P. K., and Kawamura, K.: Investigation of the tracers for plastic-enriched waste burning aerosols, *Atmospheric Environment*, 108, 49–58, <https://doi.org/10.1016/j.atmosenv.2015.02.066>, 2015.
- Kumar, V., Sahu, M., Biswal, B., Prakash, J., Choudhary, S., Raliya, R., Chadha, T. S., Fang, J., and Biswas, P.: Temporal dynamics and source characteristics of fine particulate matter using Positive Matrix Factorization (PMF), *Atmospheric Pollution Research*, 16, 102539, <https://doi.org/10.1016/j.apr.2025.102539>, 2025.
- Lack, D. A., Moosmüller, H., McMeeking, G. R., Chakrabarty, R. K., and Baumgardner, D.: Characterizing elemental, equivalent black, and refractory black carbon aerosol particles: a review of techniques, their limitations and uncertainties, *Anal Bioanal Chem*, 406, 99–122, <https://doi.org/10.1007/s00216-013-7402-3>, 2014.
- Larssen, S., Sluyter, R., and Helmis, C.: Criteria for EUROAIRNET - The EEA Air Quality Monitoring and Information Network, n.d.
- Le Berre, L., Temime-Roussel, B., Lanzafame, G. M., D’Anna, B., Marchand, N., Sauvage, S., Dufresne, M., Tinel, L., Leonardis, T., Ferreira De Brito, J., Armengaud, A., Gille, G., Lanzi, L., Bourjot, R., and Wortham, H.: Measurement report: In-depth characterization of ship emissions during operations in a Mediterranean port, <https://doi.org/10.5194/egusphere-2024-2903>, 25 September 2024.
- Le Breton, M., Hallquist, Å. M., Pathak, R. K., Simpson, D., Wang, Y., Johansson, J., Zheng, J., Yang, Y., Shang, D., Wang, H., Liu, Q., Chan, C., Wang, T., Bannan, T. J., Priestley, M., Percival, C. J., Shallcross, D. E., Lu, K., Guo, S., Hu, M., and Hallquist, M.: Chlorine oxidation of VOCs at a semi-rural site in Beijing: significant chlorine liberation from



- 925 CINO₂ and subsequent gas- and particle-phase Cl-VOC production, *Atmos. Chem. Phys.*, 18, 13013–13030, <https://doi.org/10.5194/acp-18-13013-2018>, 2018.
- Ledoux, F., Laversin, H., Courcot, D., Courcot, L., Zhilinskaya, E. A., Puskaric, E., and Aboukais, A.: Characterization of iron and manganese species in atmospheric aerosols from anthropogenic sources, *Atmospheric Research*, 82, 622–632, <https://doi.org/10.1016/j.atmosres.2006.02.018>, 2006.
- 930 Lee, B. H., Lopez-Hilfiker, F. D., Schroder, J. C., Campuzano-Jost, P., Jimenez, J. L., McDuffie, E. E., Fibiger, D. L., Veres, P. R., Brown, S. S., Campos, T. L., Weinheimer, A. J., Flocke, F. F., Norris, G., O'Mara, K., Green, J. R., Fiddler, M. N., Bililign, S., Shah, V., Jaeglé, L., and Thornton, J. A.: Airborne Observations of Reactive Inorganic Chlorine and Bromine Species in the Exhaust of Coal-Fired Power Plants, *JGR Atmospheres*, 123, <https://doi.org/10.1029/2018JD029284>, 2018.
- Lei, L., Xu, W., Lin, C., Chen, B., Fossum, K. N., Ceburnis, D., O'Dowd, C., and Ovadnevaite, J.: Enhancing Differentiation of Oxygenated Organic Aerosol: A Machine Learning Approach to Distinguish Local and Transboundary Pollution, *ACS EST Air*, 2, 891–902, <https://doi.org/10.1021/acsestair.4c00331>, 2025.
- 935 Lin, C., Ceburnis, D., O'Dowd, C., and Ovadnevaite, J.: Seasonality of Aerosol Sources Calls for Distinct Air Quality Mitigation Strategies, *Toxics*, 10, 121, <https://doi.org/10.3390/toxics10030121>, 2022.
- Liu, T., Chan, A. W. H., and Abbatt, J. P. D.: Multiphase Oxidation of Sulfur Dioxide in Aerosol Particles: Implications for Sulfate Formation in Polluted Environments, *Environ. Sci. Technol.*, 55, 4227–4242, <https://doi.org/10.1021/acs.est.0c06496>, 2021.
- 940 Liu, X., Zhang, X., Jin, B., Wang, T., Qian, S., Zou, J., Dinh, V. N. T., Jaffrezou, J.-L., Uzu, G., Dominutti, P., Darfeuil, S., Favez, O., Conil, S., Marchand, N., Castillo, S., De La Rosa, J. D., Grange, S., Hueglin, C., Eleftheriadis, K., Diapouli, E., Manousakas, M.-I., Gini, M., Nava, S., Calzolari, G., Alves, C., Monge, M., Reche, C., Harrison, R. M., Hopke, P. K., Alastuey, A., and Querol, X.: Source apportionment of PM₁₀ based on offline chemical speciation data at 24 European sites, *npj Clim Atmos Sci*, 8, <https://doi.org/10.1038/s41612-025-01097-7>, 2025.
- 945 Lu, G., Brook, J. R., Rami Alfarra, M., Anlauf, K., Richard Leaitch, W., Sharma, S., Wang, D., Worsnop, D. R., and Phinney, L.: Identification and characterization of inland ship plumes over Vancouver, BC, *Atmospheric Environment*, 40, 2767–2782, <https://doi.org/10.1016/j.atmosenv.2005.12.054>, 2006.
- 950 Manousakas, M., Furger, M., Daellenbach, K. R., Canonaco, F., Chen, G., Tobler, A., Rai, P., Qi, L., Tremper, A. H., Green, D., Hueglin, C., Slowik, J. G., El Haddad, I., and Prevot, A. S. H.: Source identification of the elemental fraction of particulate matter using size segregated, highly time-resolved data and an optimized source apportionment approach, *Atmospheric Environment: X*, 14, 100165, <https://doi.org/10.1016/j.aeaoa.2022.100165>, 2022.
- 955 Manousakas, M. I., Zografou, O., Canonaco, F., Diapouli, E., Papagiannis, S., Gini, M., Vasilatou, V., Tobler, A., Vratolis, S., Slowik, J. G., Daellenbach, K. R., Prevot, A. S. H., and Eleftheriadis, K.: Implementation of Real-Time Source Apportionment Approaches Using the ACSM-Xact-Aethalometer (AXA) Set-Up with SoFi RT: The Athens Case Study, <https://doi.org/10.5194/egusphere-2025-542>, 24 February 2025.



- Marris, H., Deboudt, K., Augustin, P., Flament, P., Blond, F., Fiani, E., Fourmentin, M., and Delbarre, H.: Fast changes in chemical composition and size distribution of fine particles during the near-field transport of industrial plumes, *Science of The Total Environment*, 427–428, 126–138, <https://doi.org/10.1016/j.scitotenv.2012.03.068>, 2012.
- Masoud, C. G., Modi, M., Bhattacharyya, N., Jahn, L. G., McPherson, K. N., Abue, P., Patel, K., Allen, D. T., and Hildebrandt Ruiz, L.: High Chlorine Concentrations in an Unconventional Oil and Gas Development Region and Impacts on Atmospheric Chemistry, *Environ. Sci. Technol.*, 57, 15454–15464, <https://doi.org/10.1021/acs.est.3c04005>, 2023.
- Massimi, L., Simonetti, G., Buiarelli, F., Di Filippo, P., Pomata, D., Riccardi, C., Ristorini, M., Astolfi, M. L., and Canepari, S.: Spatial distribution of levoglucosan and alternative biomass burning tracers in atmospheric aerosols, in an urban and industrial hot-spot of Central Italy, *Atmospheric Research*, 239, 104904, <https://doi.org/10.1016/j.atmosres.2020.104904>, 2020.
- Moffet, R. C., Desyaterik, Y., Hopkins, R. J., Tivanski, A. V., Gilles, M. K., Wang, Y., Shutthanandan, V., Molina, L. T., Abraham, R. G., Johnson, K. S., Mugica, V., Molina, M. J., Laskin, A., and Prather, K. A.: Characterization of Aerosols Containing Zn, Pb, and Cl from an Industrial Region of Mexico City, *Environ. Sci. Technol.*, 42, 7091–7097, <https://doi.org/10.1021/es7030483>, 2008.
- Momenimovahed, A., Gagné, S., Gajdosechova, Z., Corbin, J. C., Smallwood, G. J., Mester, Z., Behrends, B., Wichmann, V., and Thomson, K. A.: Effective density and metals content of particle emissions generated by a diesel engine operating under different marine fuels, *Journal of Aerosol Science*, 151, 105651, <https://doi.org/10.1016/j.jaerosci.2020.105651>, 2021.
- Morais, S., Fonseca, H. M. A. C., Oliveira, S. M. R., Oliveira, H., Gupta, V. K., Sharma, B., and De Lourdes Pereira, M.: Environmental and Health Hazards of Chromated Copper Arsenate-Treated Wood: A Review, *IJERPH*, 18, 5518, <https://doi.org/10.3390/ijerph18115518>, 2021.
- Moreno, T., Pandolfi, M., Querol, X., Lavín, J., Alastuey, A., Viana, M., and Gibbons, W.: Manganese in the urban atmosphere: identifying anomalous concentrations and sources, *Environ Sci Pollut Res*, 18, 173–183, <https://doi.org/10.1007/s11356-010-0353-8>, 2011.
- Ngoc Thuy Dinh, V., Jaffrezo, J.-L., Dominutti, P., Elazzouzi, R., Darfeuil, S., Voiron, C., Marsal, A., Socquet, S., Mary, G., Cozic, J., Coulaud, C., Durif, M., Favez, O., and Uzu, G.: Decadal trends (2013–2023) in PM10 sources and oxidative potential at a European urban supersite (Alpine Valley, Grenoble, France), <https://doi.org/10.5194/egusphere-2025-2933>, 1 July 2025.
- Paatero, P.: The Multilinear Engine: A Table-Driven, Least Squares Program for Solving Multilinear Problems, including the n-Way Parallel Factor Analysis Model, 2024.
- Paatero, P. and Hopke, P. K.: Discarding or downweighting high-noise variables in factor analytic models, *Analytica Chimica Acta*, 490, 277–289, [https://doi.org/10.1016/S0003-2670\(02\)01643-4](https://doi.org/10.1016/S0003-2670(02)01643-4), 2003.
- Paatero, P. and Hopke, P. K.: Rotational tools for factor analytic models, *Journal of Chemometrics*, 23, 91–100, <https://doi.org/10.1002/cem.1197>, 2009.



- Paatero, P. and Tapper, U.: Positive matrix factorization: A non-negative factor model with optimal utilization of error estimates of data values, *Environmetrics*, 5, 111–126, <https://doi.org/10.1002/env.3170050203>, 1994.
- Pant, P., Shi, Z., Pope, F. D., and Harrison, R. M.: Characterization of Traffic-Related Particulate Matter Emissions in a Road Tunnel in Birmingham, UK: Trace Metals and Organic Molecular Markers, *Aerosol Air Qual. Res.*, 17, 117–130, 995 <https://doi.org/10.4209/aaqr.2016.01.0040>, 2017.
- Parworth, C., Fast, J., Mei, F., Shippert, T., Sivaraman, C., Tilp, A., Watson, T., and Zhang, Q.: Long-term measurements of submicrometer aerosol chemistry at the Southern Great Plains (SGP) using an Aerosol Chemical Speciation Monitor (ACSM), *Atmospheric Environment*, 106, 43–55, <https://doi.org/10.1016/j.atmosenv.2015.01.060>, 2015.
- Pawar, P. V., Ghude, S. D., Govardhan, G., Acharja, P., Kulkarni, R., Kumar, R., Sinha, B., Sinha, V., Jena, C., Gunwani, P., 1000 Adhya, T. K., Nemitz, E., and Sutton, M. A.: Chloride (HCl/Cl^-) dominates inorganic aerosol formation from ammonia in the Indo-Gangetic Plain during winter: modeling and comparison with observations, *Atmos. Chem. Phys.*, 23, 41–59, <https://doi.org/10.5194/acp-23-41-2023>, 2023.
- Peng, X., Wang, W., Xia, M., Chen, H., Ravishankara, A. R., Li, Q., Saiz-Lopez, A., Liu, P., Zhang, F., Zhang, C., Xue, L., Wang, X., George, C., Wang, J., Mu, Y., Chen, J., and Wang, T.: An unexpected large continental source of reactive 1005 bromine and chlorine with significant impact on wintertime air quality, *National Science Review*, 8, nwaa304, <https://doi.org/10.1093/nsr/nwaa304>, 2021.
- Pernigotti, D. and Belis, C. A.: DeltaSA tool for source apportionment benchmarking, description and sensitivity analysis, *Atmospheric Environment*, 180, 138–148, <https://doi.org/10.1016/j.atmosenv.2018.02.046>, 2018.
- Pey, J., Pérez, N., Castillo, S., Viana, M., Moreno, T., Pandolfi, M., López-Sebastián, J. M., Alastuey, A., and Querol, X.: 1010 Geochemistry of regional background aerosols in the Western Mediterranean, *Atmospheric Research*, 94, 422–435, <https://doi.org/10.1016/j.atmosres.2009.07.001>, 2009.
- Pey, J., Alastuey, A., and Querol, X.: PM_{10} and $\text{PM}_{2.5}$ sources at an insular location in the western Mediterranean by using source apportionment techniques, *Science of The Total Environment*, 456–457, 267–277, <https://doi.org/10.1016/j.scitotenv.2013.03.084>, 2013.
- 1015 Polissar, A. V., Hopke, P. K., Paatero, P., Malm, W. C., and Sisler, J. F.: Atmospheric aerosol over Alaska: 2. Elemental composition and sources, *J. Geophys. Res.*, 103, 19045–19057, <https://doi.org/10.1029/98JD01212>, 1998.
- Pons, F., Alberti, T., Messori, G., Dulac, F., and Faranda, D.: Assessing Climate Change Impacts on the March 2024 Compound Floods and Saharan Dust Outbreak in Europe, *JGR Atmospheres*, 130, e2024JD042218, <https://doi.org/10.1029/2024JD042218>, 2025.
- 1020 Puygrenier, V., Lohou, F., Campistron, B., Saïd, F., Pigeon, G., Bénech, B., and Serça, D.: Investigation on the fine structure of sea-breeze during ESCOMPTE experiment, *Atmospheric Research*, 74, 329–353, <https://doi.org/10.1016/j.atmosres.2004.06.011>, 2005.



- Quivet, E., Höhener, P., Temime-Roussel, B., Dron, J., Revenko, G., Verlande, M., Lebaron, K., Demelas, C., Vassalo, L., and Boudenne, J.-L.: Underestimation of Anthropogenic Bromoform Released into the Environment?, *Environ. Sci. Technol.*, 56, 1522–1533, <https://doi.org/10.1021/acs.est.1c05073>, 2022.
- 1025 Rai, P., Furger, M., El Haddad, I., Kumar, V., Wang, L., Singh, A., Dixit, K., Bhattu, D., Petit, J.-E., Ganguly, D., Rastogi, N., Baltensperger, U., Tripathi, S. N., Slowik, J. G., and Prévôt, A. S. H.: Real-time measurement and source apportionment of elements in Delhi's atmosphere, *Science of The Total Environment*, 742, 140332, <https://doi.org/10.1016/j.scitotenv.2020.140332>, 2020a.
- 1030 Rai, P., Furger, M., Slowik, J. G., Canonaco, F., Fröhlich, R., Hüglin, C., Minguillón, M. C., Petterson, K., Baltensperger, U., and Prévôt, A. S. H.: Source apportionment of highly time-resolved elements during a firework episode from a rural freeway site in Switzerland, *Atmospheric Chemistry and Physics*, 20, 1657–1674, <https://doi.org/10.5194/acp-20-1657-2020>, 2020b.
- Rai, P., Furger, M., Slowik, J. G., Zhong, H., Tong, Y., Wang, L., Duan, J., Gu, Y., Qi, L., Huang, R.-J., Cao, J., 1035 Baltensperger, U., and Prévôt, A. S. H.: Characteristics and sources of hourly elements in PM₁₀ and PM_{2.5} during wintertime in Beijing, *Environmental Pollution*, 278, 116865, <https://doi.org/10.1016/j.envpol.2021.116865>, 2021.
- Reff, A., Eberly, S. I., and Bhave, P. V.: Receptor Modeling of Ambient Particulate Matter Data Using Positive Matrix Factorization: Review of Existing Methods, *Journal of the Air & Waste Management Association*, 57, 146–154, <https://doi.org/10.1080/10473289.2007.10465319>, 2007.
- 1040 Riandet, A., Xueref-Remy, I., Popovici, I., Lelandais, L., Armengaud, A., and Goloub, P.: Diurnal and Seasonal Variability of the Atmospheric Boundary-Layer Height in Marseille (France) for Mistral and Sea/Land Breeze Conditions, *Remote Sensing*, 15, 1185, <https://doi.org/10.3390/rs15051185>, 2023.
- Riffault, V., Arndt, J., Marris, H., Mbengue, S., Setyan, A., Alleman, L. Y., Deboudt, K., Flament, P., Augustin, P., Delbarre, H., and Wenger, J.: Fine and Ultrafine Particles in the Vicinity of Industrial Activities: A Review, *Critical Reviews in Environmental Science and Technology*, 45, 2305–2356, <https://doi.org/10.1080/10643389.2015.1025636>, 2015.
- 1045 Roy, P.-O., Bulle, C., and Deschênes, L.: Global-scale atmospheric modeling of aerosols to assess metal source-receptor relationships for life cycle assessment, *Int J Life Cycle Assess*, 24, 93–103, <https://doi.org/10.1007/s11367-018-1508-y>, 2019.
- Salameh, D., Detournay, A., Pey, J., Pérez, N., Liguori, F., Saraga, D., Bove, M. C., Brotto, P., Cassola, F., Massabò, D., 1050 Latella, A., Pillon, S., Formenton, G., Patti, S., Armengaud, A., Piga, D., Jaffrezo, J. L., Bartzis, J., Tolis, E., Prati, P., Querol, X., Wortham, H., and Marchand, N.: PM_{2.5} chemical composition in five European Mediterranean cities: A 1-year study, *Atmospheric Research*, 155, 102–117, <https://doi.org/10.1016/j.atmosres.2014.12.001>, 2015.
- Salameh, D., Pey, J., Bozzetti, C., El Haddad, I., Detournay, A., Sylvestre, A., Canonaco, F., Armengaud, A., Piga, D., Robin, D., Prevot, A. S. H., Jaffrezo, J.-L., Wortham, H., and Marchand, N.: Sources of PM_{2.5} at an urban-industrial 1055 Mediterranean city, Marseille (France): Application of the ME-2 solver to inorganic and organic markers, *Atmospheric Research*, 214, 263–274, <https://doi.org/10.1016/j.atmosres.2018.08.005>, 2018.



- Sandradewi, J., Prévôt, A. S. H., Szidat, S., Perron, N., Alfarra, M. R., Lanz, V. A., Weingartner, E., and Baltensperger, U.: Using Aerosol Light Absorption Measurements for the Quantitative Determination of Wood Burning and Traffic Emission Contributions to Particulate Matter, *Environ. Sci. Technol.*, 42, 3316–3323, <https://doi.org/10.1021/es702253m>, 2008.
- 1060 Schmale, J., Shindell, D., von Schneidemesser, E. et al. Air pollution: Clean up our skies. *Nature* 515, 335–337 (2014). <https://doi.org/10.1038/515335a>
- Scerri, M. M., Kandler, K., Weinbruch, S., Yubero, E., Galindo, N., Prati, P., Caponi, L., and Massabò, D.: Estimation of the contributions of the sources driving PM_{2.5} levels in a Central Mediterranean coastal town, *Chemosphere*, 211, 465–481, <https://doi.org/10.1016/j.chemosphere.2018.07.104>, 2018.
- 1065 Simpson, W. R., Brown, S. S., Saiz-Lopez, A., Thornton, J. A., and Von Glasow, R.: Tropospheric Halogen Chemistry: Sources, Cycling, and Impacts, *Chem. Rev.*, 115, 4035–4062, <https://doi.org/10.1021/cr5006638>, 2015.
- Solo-Gabriele, H.: Characteristics of chromated copper arsenate-treated wood ash, *Journal of Hazardous Materials*, 89, 213–232, [https://doi.org/10.1016/S0304-3894\(01\)00311-9](https://doi.org/10.1016/S0304-3894(01)00311-9), 2002.
- Stein, S. E. and Scott, D. R.: Optimization and testing of mass spectral library search algorithms for compound
1070 identification, *J. Am. Soc. Mass Spectrom.*, 5, 859–866, [https://doi.org/10.1016/1044-0305\(94\)87009-8](https://doi.org/10.1016/1044-0305(94)87009-8), 1994.
- Su, Y., Wu, D., Li, Q., Ding, X., Chen, Y., Zheng, H., Li, Y., Liu, Y., Liu, A., Wang, S., Cai, R., Wang, L., Jiang, J., Wang, T., Herrmann, H., George, C., Mellouki, A., and Chen, J.: Multiphase particle formation in industrial plumes corrects missing sulfate in the urban atmosphere, *One Earth*, 101320, <https://doi.org/10.1016/j.oneear.2025.101320>, 2025.
- Sylvestre, A., Mizzi, A., Mathiot, S., Masson, F., Jaffrezo, J. L., Dron, J., Mesbah, B., Wortham, H., and Marchand, N.:
1075 Comprehensive chemical characterization of industrial PM_{2.5} from steel industry activities, *Atmospheric Environment*, 152, 180–190, <https://doi.org/10.1016/j.atmosenv.2016.12.032>, 2017.
- Taiwo, A. M., Beddows, D. C. S., Calzolari, G., Harrison, R. M., Lucarelli, F., Nava, S., Shi, Z., Valli, G., and Vecchi, R.: Receptor modelling of airborne particulate matter in the vicinity of a major steelworks site, *Science of The Total Environment*, 490, 488–500, <https://doi.org/10.1016/j.scitotenv.2014.04.118>, 2014.
- 1080 Thornton, J. A., Kercher, J. P., Riedel, T. P., Wagner, N. L., Cozic, J., Holloway, J. S., Dubé, W. P., Wolfe, G. M., Quinn, P. K., Middlebrook, A. M., Alexander, B., and Brown, S. S.: A large atomic chlorine source inferred from mid-continental reactive nitrogen chemistry, *Nature*, 464, 271–274, <https://doi.org/10.1038/nature08905>, 2010.
- Tissari, J., Sippula, O., Torvela, T., Lamberg, H., Leskinen, J., Karhunen, T., Paukkunen, S., Hirvonen, M.-R., and Jokiniemi, J.: Zinc nanoparticle formation and physicochemical properties in wood combustion – Experiments with zinc-
1085 doped pellets in a small-scale boiler, *Fuel*, 143, 404–413, <https://doi.org/10.1016/j.fuel.2014.11.076>, 2015.
- Tobler, A. K., Skiba, A., Wang, D. S., Croteau, P., Styszko, K., Nęcki, J., Baltensperger, U., Slowik, J. G., and Prévôt, A. S. H.: Improved chloride quantification in quadrupole aerosol chemical speciation monitors (Q-ACSMs), *Atmos. Meas. Tech.*, 13, 5293–5301, <https://doi.org/10.5194/amt-13-5293-2020>, 2020.
- Tobler, A. K., Skiba, A., Canonaco, F., Močnik, G., Rai, P., Chen, G., Bartyzel, J., Zimnoch, M., Styszko, K., Nęcki, J.,
1090 Furger, M., Róžański, K., Baltensperger, U., Slowik, J. G., and Prevot, A. S. H.: Characterization of non-refractory (NR)



- PM₁ and source apportionment of organic aerosol in Kraków, Poland, *Atmos. Chem. Phys.*, 21, 14893–14906, <https://doi.org/10.5194/acp-21-14893-2021>, 2021.
- Tremper, A. H., Font, A., Priestman, M., Hamad, S. H., Chung, T.-C., Pribadi, A., Brown, R. J. C., Goddard, S. L., Grassineau, N., Petterson, K., Kelly, F. J., and Green, D. C.: Field and laboratory evaluation of a high time resolution x-ray
1095 fluorescence instrument for determining the elemental composition of ambient aerosols, *Atmos. Meas. Tech.*, 11, 3541–3557, <https://doi.org/10.5194/amt-11-3541-2018>, 2018.
- Ulbrich, I. M., Canagaratna, M. R., Zhang, Q., Worsnop, D. R., and Jimenez, J. L.: Interpretation of organic components from Positive Matrix Factorization of aerosol mass spectrometric data, *Atmospheric Chemistry and Physics*, 9, 2891–2918, <https://doi.org/10.5194/acp-9-2891-2009>, 2009.
- 1100 Valavanidis, A., Iliopoulos, N., Gotsis, G., and Fiotakis, K.: Persistent free radicals, heavy metals and PAHs generated in particulate soot emissions and residue ash from controlled combustion of common types of plastic, *Journal of Hazardous Materials*, 156, 277–284, <https://doi.org/10.1016/j.jhazmat.2007.12.019>, 2008.
- Via, M., Chen, G., Canonaco, F., Daellenbach, K. R., Chazau, B., Chebaicheb, H., Jiang, J., Keernik, H., Lin, C., Marchand, N., Marin, C., O'Dowd, C., Ovadnevaite, J., Petit, J.-E., Pikridas, M., Riffault, V., Sciare, J., Slowik, J. G.,
1105 Simon, L., Vasilescu, J., Zhang, Y., Favez, O., Prévôt, A. S. H., Alastuey, A., and Cruz Minguillón, M.: Rolling vs. seasonal PMF: real-world multi-site and synthetic dataset comparison, *Atmos. Meas. Tech.*, 15, 5479–5495, <https://doi.org/10.5194/amt-15-5479-2022>, 2022.
- Viana, M., Reche, C., Amato, F., Alastuey, A., Querol, X., Moreno, T., Lucarelli, F., Nava, S., Calzolari, G., Chiari, M., and Rico, M.: Evidence of biomass burning aerosols in the Barcelona urban environment during winter time, *Atmospheric
1110 Environment*, 72, 81–88, <https://doi.org/10.1016/j.atmosenv.2013.02.031>, 2013.
- Visser, S., Slowik, J. G., Furger, M., Zotter, P., Bukowiecki, N., Canonaco, F., Flechsig, U., Appel, K., Green, D. C., Tremper, A. H., Young, D. E., Williams, P. I., Allan, J. D., Coe, H., Williams, L. R., Mohr, C., Xu, L., Ng, N. L., Nemitz, E., Barlow, J. F., Halios, C. H., Fleming, Z. L., Baltensperger, U., and Prévôt, A. S. H.: Advanced source apportionment of size-resolved trace elements at multiple sites in London during winter, *Atmos. Chem. Phys.*, 15, 11291–11309,
1115 <https://doi.org/10.5194/acp-15-11291-2015>, 2015a.
- Visser, S., Slowik, J. G., Furger, M., Zotter, P., Bukowiecki, N., Dressler, R., Flechsig, U., Appel, K., Green, D. C., Tremper, A. H., Young, D. E., Williams, P. I., Allan, J. D., Herndon, S. C., Williams, L. R., Mohr, C., Xu, L., Ng, N. L., Detournay, A., Barlow, J. F., Halios, C. H., Fleming, Z. L., Baltensperger, U., and Prévôt, A. S. H.: Kerb and urban increment of highly time-resolved trace elements in PM₁₀, PM_{2.5} and
1120 PM_{1.0}; winter aerosol in London during ClearfLo 2012, *Atmos. Chem. Phys.*, 15, 2367–2386, <https://doi.org/10.5194/acp-15-2367-2015>, 2015b.
- Wang, H., Wang, X., Yang, X., Li, W., Xue, L., Wang, T., Chen, J., and Wang, W.: Mixed Chloride Aerosols and their Atmospheric Implications: A Review, *Aerosol Air Qual. Res.*, 17, 878–887, <https://doi.org/10.4209/aaqr.2016.09.0383>, 2017.



- 1125 Wang, H., Yuan, B., Zheng, E., Zhang, X., Wang, J., Lu, K., Ye, C., Yang, L., Huang, S., Hu, W., Yang, S., Peng, Y., Qi, J., Wang, S., He, X., Chen, Y., Li, T., Wang, W., Huangfu, Y., Li, X., Cai, M., Wang, X., and Shao, M.: Formation and impacts of nitryl chloride in Pearl River Delta, *Atmos. Chem. Phys.*, 22, 14837–14858, <https://doi.org/10.5194/acp-22-14837-2022>, 2022.
- Wang, X., Bi, X., Li, H., Zhang, W., Dai, Q., Song, L., Li, L., Wu, J., Zhang, Y., and Feng, Y.: The role of sources and meteorology in driving PM_{2.5}-bound chlorine, *Journal of Hazardous Materials*, 441, 129910, <https://doi.org/10.1016/j.jhazmat.2022.129910>, 2023.
- 1130 Wasson, S. J., Linak, W. P., Gullett, B. K., King, C. J., Touati, A., Huggins, F. E., Chen, Y., Shah, N., and Huffman, G. P.: Emissions of Chromium, Copper, Arsenic, and PCDDs/Fs from Open Burning of CCA-Treated Wood, *Environ. Sci. Technol.*, 39, 8865–8876, <https://doi.org/10.1021/es050891g>, 2005.
- 1135 Weber, S., Salameh, D., Albinet, A., Alleman, L. Y., Waked, A., Besombes, J.-L., Jacob, V., Guillaud, G., Meshbah, B., Rocq, B., Hulin, A., Dominik-Sègue, M., Chrétien, E., Jaffrezo, J.-L., and Favez, O.: Comparison of PM₁₀ Sources Profiles at 15 French Sites Using a Harmonized Constrained Positive Matrix Factorization Approach, *Atmosphere*, 10, 310, <https://doi.org/10.3390/atmos10060310>, 2019.
- Wen, H. and Carignan, J.: Reviews on atmospheric selenium: Emissions, speciation and fate, *Atmospheric Environment*, 41, 7151–7165, <https://doi.org/10.1016/j.atmosenv.2007.07.035>, 2007.
- 1140 Yu, G., Zhang, Y., Yang, F., He, B., Zhang, C., Zou, Z., Yang, X., Li, N., and Chen, J.: Dynamic Ni/V Ratio in the Ship-Emitted Particles Driven by Multiphase Fuel Oil Regulations in Coastal China, *Environ. Sci. Technol.*, 55, 15031–15039, <https://doi.org/10.1021/acs.est.1c02612>, 2021.
- Zhuang, H., Chan, C. K., Fang, M., and Wexler, A. S.: Formation of nitrate and non-sea-salt sulfate on coarse particles, *Atmospheric Environment*, 33, 4223–4233, [https://doi.org/10.1016/S1352-2310\(99\)00186-7](https://doi.org/10.1016/S1352-2310(99)00186-7), 1999.
- 1145 Zittis, G., Almazroui, M., Alpert, P., Ciais, P., Cramer, W., Dahdal, Y., Fnais, M., Francis, D., Hadjinicolaou, P., Howari, F., Jrrar, A., Kaskaoutis, D. G., Kulmala, M., Lazoglou, G., Mihalopoulos, N., Lin, X., Rudich, Y., Sciare, J., Stenchikov, G., Xoplaki, E., and Lelieveld, J.: Climate Change and Weather Extremes in the Eastern Mediterranean and Middle East, *Reviews of Geophysics*, 60, e2021RG000762, <https://doi.org/10.1029/2021RG000762>, 2022.
- 1150